China Geology 8 (2025) 389−407

China Geology

Journal homepage: http://chinageology.cgs.cn
https://www.sciencedirect.com/journal/china-geology

# Accumulation process and potential of Jurassic tight sandstone oil and gas in Eastern Yangxia sag of Kuqa Depression

Cai-yuan Dong[a,*], Liang Zhang[b], Wei Yang[a], Zhen-ping Xu[b], Jun Li[a], Wei-dong Miao[a]

[a] *Research Institute of Petroleum Exploration and Development of PetroChina*, *Beijing* 100083, *China*
[b] *PetroChina Tarim Oilfield Campany*, *Kolar* 841000, *China*

ARTICLE INFO

*Article history:*
Received 4 July 2023
Received in revised form 23 October 2023
Accepted 24 November 2023
Available online 25 April 2025

*Keywords:*
Oil and gas source
Densification time
Accumulation process
Tight oil and gas potential
Jurassic
Yangxia sag
Kuqa Depression

ABSTRACT

The Jurassic tight sandstone oil and gas exploration and development in the eastern Yangxia Sag is a new field. To elucidate the origin, accumulation process and potential of tight oil and gas, the authors have conducted comprehensive analyses employing methodologies encompassing source rocks, oil geochemistry, and fluid inclusions. The results show that the abundance of organic matter of Jurassic source rocks is high, and the type of organic matter is of II-III and in mature evolution stage. The main source rocks of oil and gas are Huangshanjie Formation and Jurassic coal-bearing source rocks. Ahe Formation developed two stages of hydrocarbon charging, and the period is later than the reservoir densification time. Yangxia Formation oil charged before the reservoir densified, and the late gas charged after the reservoir densified. Hydrocarbon generation intensity of Jurassic source rocks has reached the basic conditions for the formation of tight gas reservoirs. Controlled by the difference of source rocks distribution and accumulation process, tight sandstone oil and gas accumulation conditions are better in the depression direction than in the southeast margin area. This study is of practical importance for expanding the exploration field and selecting favorable areas in the eastern Yangxia sag.



## 1. Introduction

Tight oil and gas refer to a class of oil and gas resources occurring in non-hydrocarbon source rock systems such as clastic rock and carbonate rock with air permeability less than $1\times10^{-3}$ μm$^2$, which is considered as a key resource supporting the future development of the oil and gas industry (Zou CN et al., 2018; Sun LD et al., 2023). Tight sandstone gas is an unconventional natural gas resource type widely explored and developed worldwide especially plays an important role in China (Law BE, 2002; Jarvie DM, 2012; Feng JW et al., 2020; Guo XB et al., 2022). With the deepening geological theory of tight oil exploration and breakthroughs in key technologies such as horizontal wells and large-scale hydraulic fracturing, China's tight oil resources have great potential and recent have made positive progress, showing good prospects for development. China's exploration and development of tight oil started late and has seen rapid development. The national tight oil geological resources are distributed in the range of $12.5\times10^9$–$24.3\times10^9$ t, recoverable resources are $1.3\times10^9$–$1.806\times10^9$ t, and proved reserves are about $0.3\times10^9$ t (Sun LD, et al., 2019; Tao SZ et al., 2023).

The mechanism of tight gas accumulation has been studied extensively. Tight sandstone gas reservoirs include "continuous" tight gas reservoirs, as well as structural or trap tight gas reservoirs. The former source rocks and reservoirs adjacent to each other or interbedded distribution, natural gas close accumulation, such as the Pisens Basin of the United States, Xinchang Gas Field of western Sichuan, Sulige Gas Field (Tong XG et al., 2012; Dai JX et al., 2012). The latter is generally characterized by long-distance separation of source rocks and reservoirs. Natural gas needs to be migrated and charged under the communication of faults and faults to form reservoirs, such as Dabei-Keshen Gas Field in Kuqa Depression (Dai JX et al., 2012; Jia AL et al., 2022). Different types of tight sandstone gas reservoirs have different natural gas charging and accumulation processes, which will eventually lead to significant differences in gas-water

First author: *E-mail address*: dongcn69@163.com (Cai-yuan Dong).

* Corresponding author: *E-mail address*: dongcn69@163.com (Cai-yuan Dong).

Literary editor: Li-qiong Jia
doi:10.31035/cg2023063
2096-5192/© 2025 China Geology Editorial Office.

distribution and directly affect the development effect (Law BE, 2002; Guo XB et al., 2019; Ni LT et al., 2022). After years of exploration and development, the original resource potential is insufficient, so it is necessary to expand new areas of exploration and development in Kuqa Depression. In recent years, Yangxia Sag is the key area of Jurassic oil and gas exploration to the southeast, which are close to the hydrocarbon generation center and have superior hydrocarbon source conditions. The exploration deployment changed from the early structural reservoir to the lithological stratigraphic reservoir in the gentle slope zone. For example, Well YX-2 drilled in the south gentle slope zone and Well YT-1 drilled in the north gentle slope zone, etc., the lithological stratigraphic traps of Jurassic Yangxia Formation and Ahe Formation encountered by drilling. Well YT-1 was tested in Ahe Formation, with only a small amount of oil and gas was produced. Overall, the oil test results are not ideal, the reason is not clear. This is very unfavorable to the exploration and development of Jurassic oil and gas in Yangxia Sag. Therefore, based on the experimental analysis of source rock, crude oil geochemistry, reservoir diagenetic evolution and fluid inclusion, this paper aims to find out the source of Jurassic oil and gas, the main source rock and the relationship between reservoir densification process and accumulation time series, etc., to reveal the process of Jurassic oil and gas charging. It provides geological basis for further oil and gas exploration and development deployment in Kuqa Depression.

## 2. Geological setting

Kuqa Depression, located in the northern part of Tarim Basin, is a superimposed foreland basin mainly composed by Mesozoic-Cenozoic sediments, with the southern Tianshan Mountains in the north margin and the Tabei uplift in the south (Figs. 1a, b). It is distributed in a NEE-trending strip, with an east-west length of about 550 km and a north-south width of 30–80 km, and the exploration area is 28000 km$^2$ (Jia D et al., 1997; Lu YH et al., 2015; Guo XW et al., 2016). It is one of the main fields of natural gas exploration and development in China. Kuqa Depression is adjacent to the Tianshan fold belt and can be divided into the northern monocline belt, Kelasu thrust belt, Yiqikeli thrust belt, Qiuritage thrust belt, southern slope belt, Wushi depression, Baicheng depression and Yangxia sag and other secondary tectonic units (Liu JL et al., 2016; Wan JL et al. 2022). Among them, Yangxia Sag is the key area of Kuqa Depression oil and gas exploration and development, and the study area is in the east of Yangxia sag (Fig. 1c). Source rocks are mainly developed in Mesozoic Triassic and Jurassic (Fig. 1d). Among them, Triassic Huangshanjie Formation ($T_3h$) and Jurassic Qiakemake Formation ($J_2q$) are lacustrine source rocks, Yangxia Formation ($J_1y$) and Kezilenuer Formation ($J_2kz$) are coal-measure source rocks (Fig. 1d) (Li F et al., 2015; Zhao HT et al., 2022).

## 3. Samples and experimental methods

### 3.1. Samples

The core of the sample was taken from YT-1 and YX-2, the key Wells in the eastern part of the Yangxia sag. (Fig. 2). A series of experiments were carried out to analyze the Triassic and Jurassic source rocks and reservoir samples from Well YT-1 and Well YX-2 in the eastern part of Yangxia sag. The experimental analysis items include total organic carbon (TOC) of source rocks, rock pyrolysis and saturated hydrocarbon chromatography-mass spectrometry of crude oil and source rock extracts, etc. The conventional experimental analysis of cast thin sections and fluid inclusions was carried out for sandstone reservoir sections of the Yangxia Formation and Ahe Formation. Reservoir physical properties and source rock vitrinite reflectance ($R_o$) measurements were collected from the company units for the two wells.

### 3.2. Experimental methods

#### 3.2.1. Total organic carbon (TOC)

Weigh 80–120 mg samples into the crucible and add hydrochloric acid (the volume ratio of hydrochloric acid to distilled water is 1∶7) to remove inorganic carbon in the sample. After the reaction stops completely (no obvious bubbles appear), add distilled water to rinse residual hydrochloric acid to make the pH of the sample neutral, and then dry it at low temperature. Total organic carbon content (TOC) was analyzed by LECO-CS230 carbon and sulfur analyzer. The experimental process was based on the national standard of "Determination of organic carbon in Sedimentary rocks, GB/T 19145-2022".

#### 3.2.2. Pyrolysis of rock

The powder sample of about 100 mg was weighed, placed in the pyrolysis crucible, and washed with nitrogen heated to 90°C for 2 min. The light hydrocarbons in the sample were blown into the hydrogen flame detector, and the $S_0$ peak was measured, which was often very low and could be ignored. Then the sample was rapidly heated to 300°C and kept at constant temperature for 3 min, and the content of $S_1$ in the sample was measured. The temperature was raised from 300°C to 600°C at a rate of 25 °C/min, and the temperature was constant for 1 min to determine the content of $S_2$. The rock pyrolysis analysis was performed by OGE-II oil and gas evaluation workstation, and the experimental process was based on the national standard of "Rock Pyrolysis Analysis, GB/T 18602-2012".

#### 3.2.3. Gas chromatography-mass spectrometry (GC-MS)

Gas chromatography-mass spectrometry (GC-MS) analysis of saturated hydrocarbon: After surface decontamination and drying, the source rock samples were crushed to 200 mesh, Soxhlet extraction method was used for 72 hours of chloroform extraction to obtain chloroform asphalt. The chloroform asphalt or crude oil samples extracted

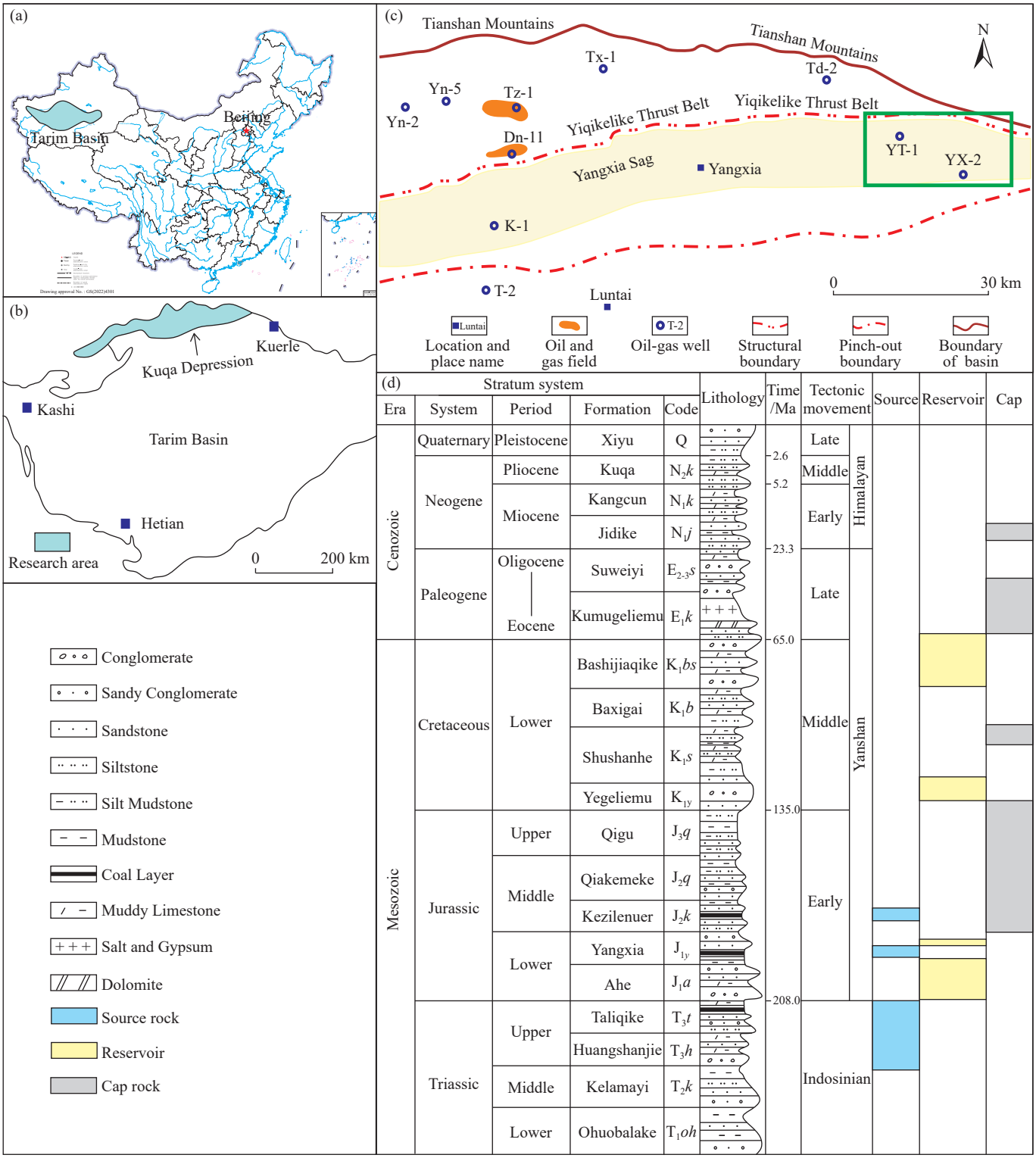


**Fig. 1.** Position of the research region and stratigraphic composite histogram in Kuqa Depression (modified from Liu JL et al., 2016; Wan JL et al. 2022).

from the source rock were separated by column chromatography, and the separated saturated hydrocarbon components were analyzed by chromatography-mass spectrometry using HP GC6890/5973MSD gas chromatography-mass spectrometry.

*3.2.4. Fluid inclusion experiments*

The main instruments used for reservoir fluid inclusion testing are Nikon 80i Nikon microscope and HMGS600 hot and cold table, and the temperature range is −196°C – 600°C. Firstly, the inclusion light plate was placed under a low power microscope, and the phase, appearance and distribution characteristics of the inclusion were observed under the transmitted light. The fluorescence characteristics of fluid inclusions were observed under fluorescence, oil

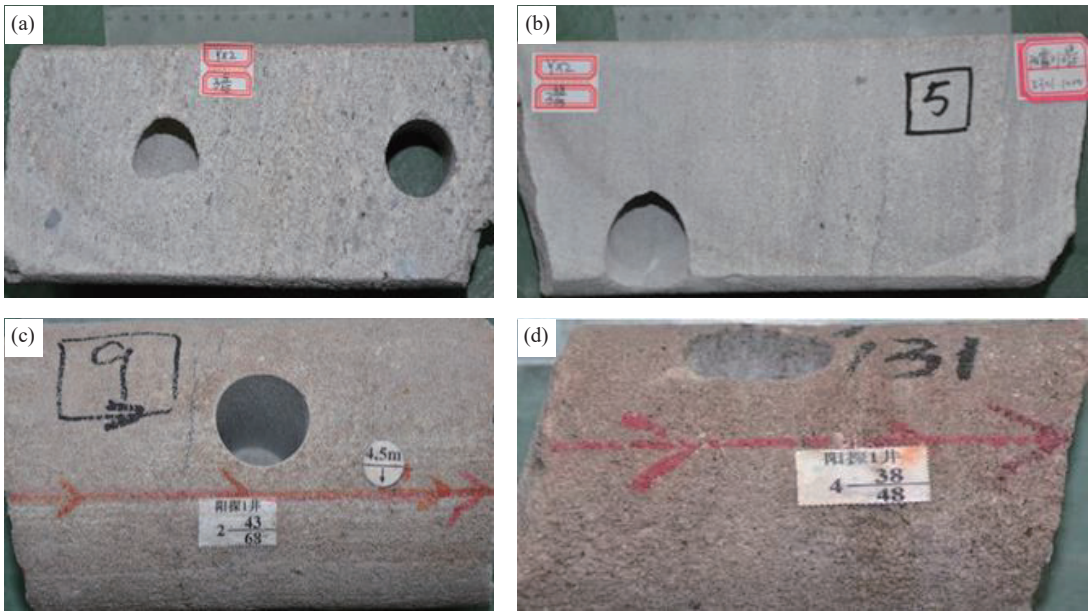


**Fig. 2.** Core samples from Yangxia Formation and Ahe Formation in Yangxia sag. a–Well YX-2, 5290.3 m, $J_1y$, gravelly coarse sandstone; b–Well YX-2, 5301.1 m, $J_1y$, coarse-medium sandstone with positive grain sequence; c–Well YT-1, 7712.2 m, $J_1a$, grey thick medium sandstone; d–Well YT-1, 7798.4 m, $J_1a$, gray sand-bearing coarse grained rock.

(hydrocarbon) inclusions and brine inclusions were distinguished, and the homogenization temperature of their associated brine inclusions was determined respectively. The homogenization temperature was measured by means of a hot and cold table and a polarizing microscope equipped with a long focal length objective. Firstly, the temperature and freezing point of the instrument were calibrated, and then the segmented light sheet of appropriate size was placed in the sample chamber of the hot and cold platform to observe and select the salt water inclusions associated with hydrocarbon inclusions which could be used for temperature measurement. At the heating rate of 5–10°C/min, when the inclusions are heated to a certain temperature, the two or more phases of the phase transition to a phase, the temperature at this time is the homogenization temperature (Th), and the measurement error is ±0.1 °C.

## 4. Results and analysis

### *4.1. Geochemical characteristics of source rocks*

#### *4.1.1. Abundance of organic matter*

The abundance of organic matter of source rocks is the basic index to evaluate the hydrocarbon generation performance. Different types of source rocks have different evaluation criteria. Based on a large amount of geochemical data of source rocks in western China, the evaluation criteria for organic matter abundance of lacustrine source rocks and coal-measure source rocks were established (Chen JP et al., 1997). However, these two evaluation criteria are mainly used to evaluate the oil generation capacity of the source rock, and the gas generation capacity of the source rock has not been fully considered.

The source rocks of Huangshanjie Formation and Qiakemake Formation in the study area are mainly mudstones, which are developed in a lacustrine sedimentary environment. The maximum TOC of mudstone in Huangshanjie Formation is 8.8%, the minimum is 0.7%, and the average is 2.74%. The maximum value of hydrocarbon generation potential ($S_1$+$S_2$) was 12.8 mg/g, the minimum value was 0.2 mg/g and the average value was 3.14 mg/g. TOC of mudstones in the Qiakemake Formation is lower than 1.0% and $S_1$+$S_2$ is lower than 2.0 mg/g (Fig. 3a). Based on the Chinese continental lacustrine mudstone proposed by Huang DF (1982) as the evaluation criterion of oil source rocks, the mudstone samples of Huangshanjie Formation belong to the good and very good grade, accounting for about 85.4% of the total samples, while the mudstone samples of the Qiakemake Formation are very few and most of them are poor and non-source rocks, which may not be representative (Fig. 3a). Coal measure source rocks are developed in the Triassic Taliqike Formation, Jurassic Yangxia Formation and Kezilenur Formation, which can be divided into mudstone, carbonaceous mudstone, and coal according to lithology classification. However, drilling reveals that the thickness of coal seam and carbonaceous mudstone is very small, and mudstone is the most developed. TOC of the mudstones in the Taliqike Formation ranges from 0.9% to 2.6%, with an average of 1.7%. The distribution of $S_1$+$S_2$ ranges from 0.7 mg/g to 4.7 mg/g, with an average of 2.4 mg/g. TOC of mudstones in Yangxia Formation ranges from 0.2% to 4.1%, with an average of 1.1%. The distribution of $S_1$+$S_2$ ranges from 0.2–8.8 mg/g, with an average of 1.9 mg/g. TOC of mudstones in Kezilenur Formation ranges from 0.1%–4.8%, with an average of 1.1%. The distribution of $S_1$+$S_2$ ranges from 0.4–4.7 mg/g, with an average of 2.0 mg/g. According to the evaluation criteria of coal measure oil source rocks (Chen JP et al., 1997), mudstone samples of Taliqike Formation ($T_3t$) basically reach the standards of medium source rocks

(Fig. 3b). In addition, 34.3% of mudstone samples from the Yangxia Formation and 45.5% of mudstone samples from the Kezilenur Formation meet the standard of medium oil source rocks. The rest of the samples are mostly poor and non-hydrocarbon source rocks, and few good source rocks (Fig. 3b).

TOC values of the carbonaceous mudstones of Yangxia and Kizilenur formations are generally high, ranging from 6.4% to 39.0%. In the evaluation of organic matter abundance, the potential hydrocarbon generation by rock pyrolysis ($S_1$+$S_2$) should be mainly referred. The value of $S_1$+$S_2$ ranges from 11.5–63.5 mg/g, with an average value of 32.0 mg/g, generally reaching the evaluation standard of medium source rocks. There is no unified evaluation standard for coal rock, but its TOC value and hydrocarbon generation potential value are very high. Coal rock has a strong hydrocarbon generation capacity, but the adsorption capacity of hydrocarbons is stronger, whether it can be used as an effective source rock to discharge hydrocarbons predecessors have different views. In view of the thin thickness of the coal rocks in the study area and their small contribution to hydrocarbon supply, the evaluation of the coal rocks as source rocks will not be further discussed in this paper.

*4.1.2. Types of organic matter*

In the intersection diagram of rock pyrolysis $T_{max}$ and hydrogen index (HI=100×$S_2$/TOC), the organic matter types of the experimental samples of Triassic and Jurassic source rocks are mainly type III, and some are type $II_1$ (Fig. 4). In general, the hydrogen index of mudstone samples of Huangshanjie Formation is low, with an average of 108 mg/g TOC. Some samples are type $II_1$-$II_2$ kerogen, which has strong oil-generating capacity (Fig. 4a). Mudstone samples of the Qiakemake Formation are small, and the hydrogen index is generally low, with an average of 64.0 mg/g TOC, all of which are type III kerogen (Fig. 4a). The mudstone of Taliqike Formation has a low hydrogen index, ranging from 11–161 mg/g TOC with an average of 74.4 mg/g TOC, corresponding type III kerogen (Fig. 4b). For Yangxia Formation and Kezilenur Formation mudstone samples, hydrogen index of some samples is high, and about 24.3% of the samples is higher than 200mg/g TOC, corresponding type $II_2$–$II_1$ kerogen, which has certain oil generating capacity (Fig. 4b). The kerogen types of carbonaceous mudstone and coal are mainly III–$II_2$ (Fig. 4c).

*4.1.3. Maturity of organic matter*

There are many methods to evaluate the maturity of organic matter in source rocks, and vitrinite reflectance ($R_o$, %) is the most used parameter. The measured data show that the source rock $R_o$ of the Triassic Huangshanjie Formation ranges from 0.99% to 1.38%. The $R_o$ of Taliqike Formation ranges from 0.96% to 1.39%. The source rock $R_o$ of Jurassic

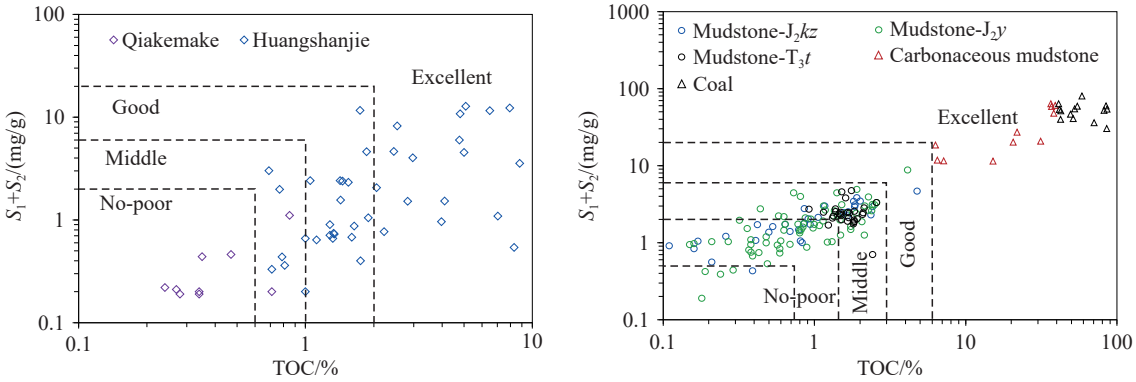


**Fig. 3.** Relationship between TOC and ($S_1$+$S_2$) of Triassic-Jurassic source rocks in Yangxia sag.

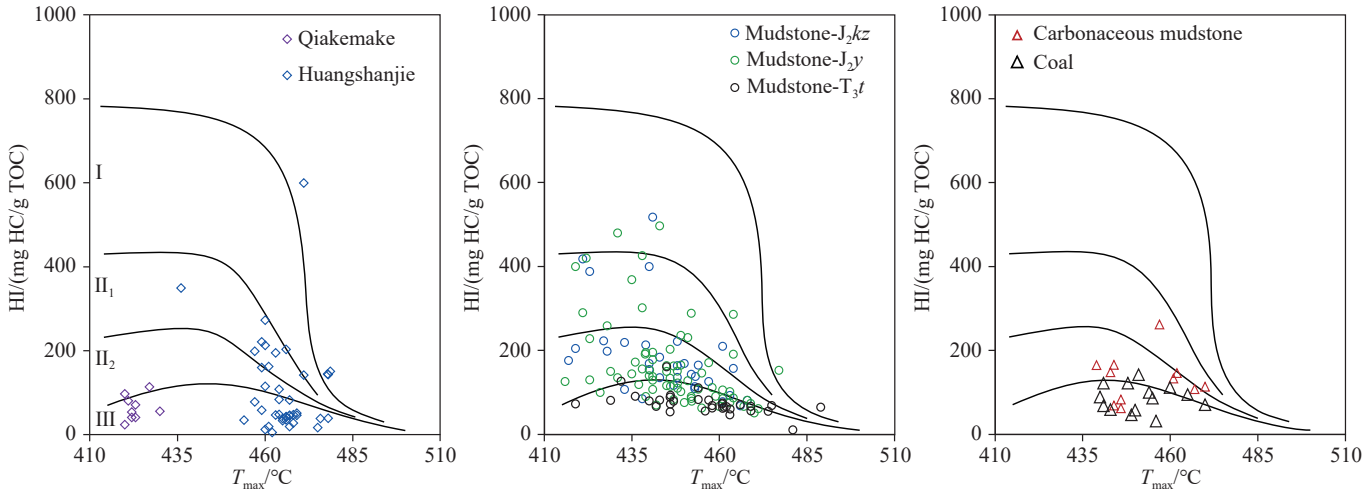


**Fig. 4.** Kerogen type identification of source rocks with different strata and different lithologies in Yangxia sag.

Yangxia Formation ranges from 0.98% to 1.10%. The hydrocarbon source rock $R_o$ of Kizilenur Formation ranges from 0.99% to 1.15%. In general, the source rocks $R_o$ of the Triassic and Jurassic in Yangxia Sag ranges from 0.96% to 1.38%, and they are in the mature evolution stage. Only part of the Triassic source rocks has reached the early stage of high maturity.

In deep oil and gas exploration, the hydrocarbon generation capacity of source rocks is one of the key prerequisites for controlling the oil and gas bearing capacity of deep reservoirs. Deep source rocks have a large hydrocarbon yield, so deep reservoirs have a high probability of producing rich oil and gas. On the contrary, it is small and the exploration risk is increased. Therefore, it is important to determine the lower limit of the hydrocarbon production depth of the source rock or kerogen. Based on summarizing previous achievements, Du SH et al., (2023) studied the lower limit of hydrocarbon generation depth by the equations with clear physical significance, and pointed out that the lower limit of hydrocarbon generation of kerogen ranges from 2539 m to 16337 m, with an average of 6926 m. The source rocks involved in this paper are all within the range of effective hydrocarbon generation depth, so they can be used as potential source rocks. It is necessary to judge which set of source rocks is the main one based on the results of oil and gas source correlation.

### *4.2. Biomarkers characteristics of source rocks and oil*

#### *4.2.1. Biomarkers characteristics of source rocks*

Typical biomarker characteristics of source rocks in the Triassic Huangshanjie Formation are shown in Fig. 5a and b. The tricyclic terpanes series show normal distribution with $C_{20}$ or $C_{21}$ as the highest main peak, but the content of $C_{19}$ tricyclic terpanes is relatively low, indicating that the input of terrestrial higher plants in organic matter is limited (Dutta S et al., 2006; Philp P et al., 2021). The abundance of $C_{24}$ tetracyclic terpanes ($C_{24}$Tet) is high, and $C_{24}$Tet/$C_{26}$ tetracyclic terpanes ($C_{24}$Tet/$C_{26}$TT) is between 1.0 and 2.0, indicating that there is a certain amount of terrestrial organic matter input in the lake basin, but it is not significant (Kruge MA et al., 1996; Samuel OJ et al., 2010). The higher the Gammacerane index (Gammacerane / $C_{30}$ hopane) value, the higher the salinity of the sedimentary water (Zhu YM et al., 2005). The source rock of Huangshanjie Formation has a medium content of gammacerane and Gammacerane index greater than 0.3, reflecting the medium salinity of the sedimentary water and which is conducive to the deposition and preservation of low aquatic organic matter. The $C_{27}$-$C_{28}$-$C_{29}$ regular steranes have a “V” type distribution, and the $C_{29}$ regular steranes are slightly higher than the $C_{27}$ regular steranes. Therefore, the source rocks of Huangshanjie Formation formed in brackish sedimentary environment, the organic matter source compositions of the lower and middle aquatic org anisms contributed more, and some of them were terrigenous higher plants. Generally, it has the characteristics of sapropelic organic matter.

The biomarker characteristics of saturated hydrocarbon reflect that the sedimentary water environment of the source rocks of the Jurassic Qiakemake Formation has changed to some extent. The tricyclic terpanes in most of the source rocks are dominated by $C_{19}$, showing a stepwise distribution with decreasing abundance (Fig. 5c and d). $C_{24}$Tet are abundant, with $C_{24}$Tet/$C_{26}$TT ranging from 1.0 to 2.0, indicating a large contribution of terrigenous organic matter (Hao F et al., 2012). Gammacerane index is greater than 0.8, indicating a high salinity water environment. In addition, the most striking feature of this type of source rock is the high content of rearranged compounds. For example, the abundance of $C_{30}$ rearranged hopanes is even higher than that of $C_{30}$ hopanes, and $C_{30}$ rearranged hopanes / $C_{30}$ hopanes can be up to 2.0. $C_{30}$ rearranged hopanes generally come from sediments that are weakly oxidized to oxidizing environments. The catalytic effect of clay minerals contributes to the formation of rearranged hopanes (Moldowan JM et al., 1991； Zhu YM et al., 2007; Jiang L and Zhang RH, 2015). The regular $C_{27}$- $C_{28}$-$C_{29}$ steranes have a “V” type distribution, and $C_{29}$ steranes are slightly higher than $C_{27}$ steranes. Although the sedimentary water environment of the hydrocarbon source rocks of the Qiakemake Formation in Yangxia Sag has changed to some extent, the source structure of organic matter is basically the same. Both terrestrial higher plants and lower organisms contribute to the source of organic matter, which is a mixed type of organic matter.

The molecular geochemical characteristics of source rocks of Yangxia Formation (Fig. 5e) and Kezilenur Formation (Fig. 5f) are similar. In the coal measure source rocks of Yangxia Formation, $C_{20}$ is the main peak of tricyclic terpane series, and $C_{24}$-$C_{26}$ tetracyclic terpane series are well distributed with high content, indicating that terrigenous higher plants contribute more to the source rocks. The gammacerane content is extremely low, reflecting a low salt, shallow water environment. The regular steranes are dominated by $C_{29}$ steranes, which are generally reverse “L” (Fig. 5e), reflecting extremely rich terrestrial input characteristics.

The biomarker characteristics of some source rocks are that the tricyclic terpane series show a stepwise decrease trend of $C_{19} > C_{20} > C_{21}$, and the content of $C_{24}$ tetracyclic terpane is higher, which indicates more abundant terrestrial organic matter input. There is a certain gammacerane. Regular steranes show an irregular near “inverse L” distribution, and $C_{27}$ steranes are slightly smaller than $C_{29}$ steranes (Fig. 5f). The above characteristics indicate that the source rocks of Yangxia Formation and Kezilenur Formation have a large contribution of terrigenous organic matter. A small amount of coal seams and carbonaceous mudstones are also developed in the Taliqike Formation. The tricyclic terpanes in the biomarker compounds are mainly $C_{21}$, and $C_{20}$, $C_{21}$, and $C_{23}$ tricyclic terpanes show a gradual increasing trend (Fig. 5g). The gammacerane index is about 0.20, and the $C_{27}$-$C_{28}$-$C_{29}$ regular steranes are distributed in the “V” type, which belongs to the lacustrine facies deposit (Fig. 5g). The high content of

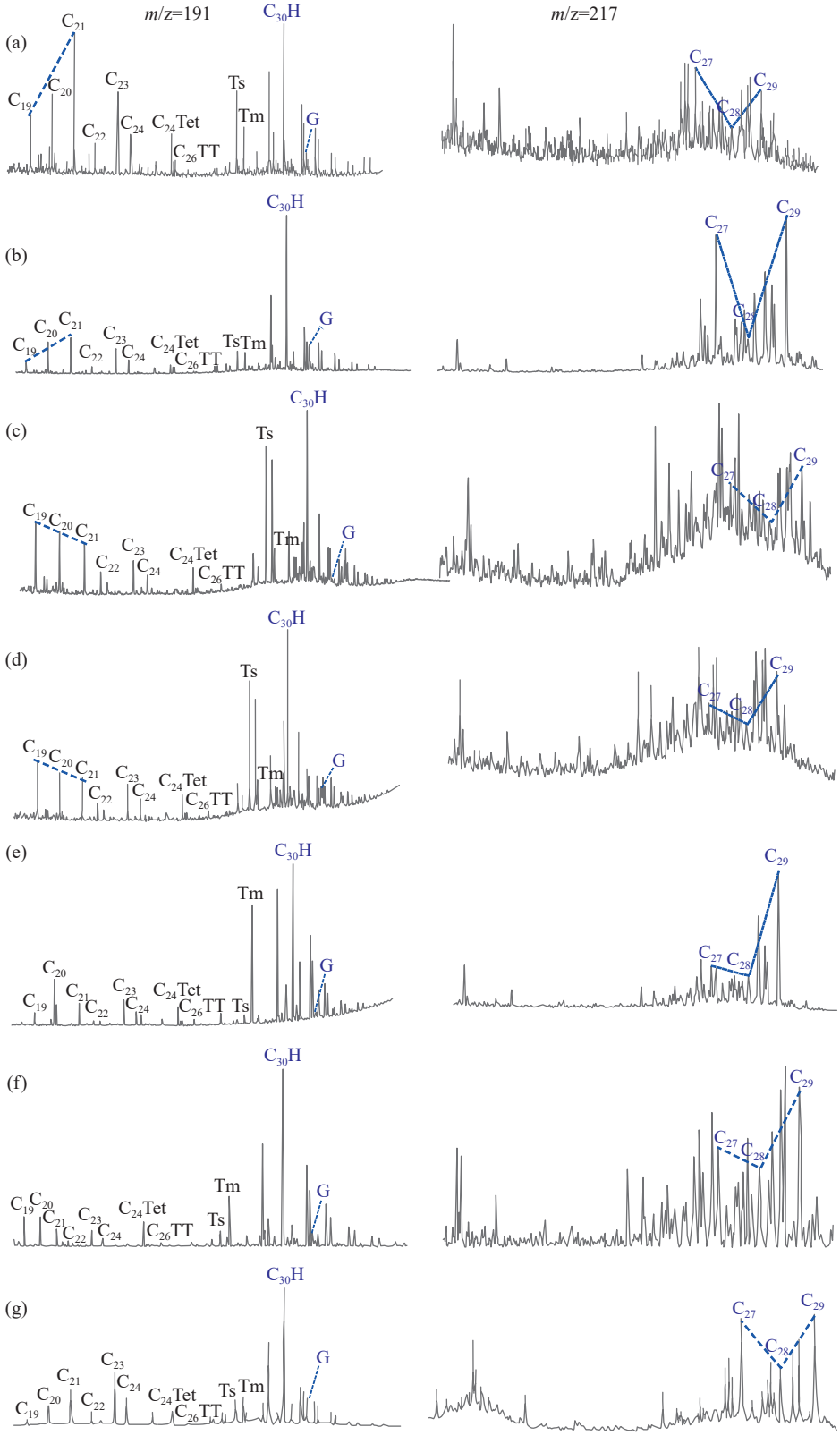


**Fig. 5.** Characteristics of terpanes (m/z=191) and steranes (m/z=217) in Triassic and Jurassic source rocks. Note: $C_{24}$Tet, $C_{24}$ tetracyclic terpanes; $C_{26}$ TT, $C_{26}$ tetracyclic terpanes; $C_{30}$H, $C_{30}$ hopanes; D, $C_{30}$ rearranged hopanes; G, gammacerane. a, b–Mudstone, Triassic Huangshanjie Formation; c, d–mudstone, Jurassic Qiakemake Formation; e–Carbonaceous mudstone, Jurassic Yangxia Formation; f–mudstone, Jurassic Kezilenur Formation; g–mudstone, Triassic Taliqike Formation.

gammacerane is an important symbol of the phase distinction between the mudstone of the Taliqike Formation and the coal source rocks of the Yangxia Formation and the Kezilenur Formation.

*4.2.2. Biomarkers characteristics of crude oil and oil source*

The crude oil or oil sand samples of well YX-2 and well YT-1 in the study area were analyzed by saturated hydrocarbon chromatography-mass spectrometry. It is found

that the content of $C_{24}$Tet is higher in the crude oil (oil sandstone extract) samples of well YX-2, and the gammacerane index is less than 0.1, and the content of rearranged hopane is lower. The $C_{29}$ regular sterane is slightly higher than the $C_{27}$ regular sterane, which is approximately inverted "L" type, and tricyclic terpane $C_{19}<C_{20}<C_{21}$ (Fig. 6). It indicates that the source oil of well YX-2 is the source rock of Yangxia Formation and Kizilenur Formation, and there may be a small amount of contribution from the source rock of Huangshanjie Formation. The content of tricyclic terpanes in the mixed crude oil of Yangxia Formation and Ahe Formation in well YT-1 is higher, $C_{19}>C_{20}>C_{21}$. The content of $C_{27}$ regular steranes and $C_{29}$ regular steranes in regular steranes is similar, which is like "V" type and the content of gammacerane is higher. According to the characteristics of biostandard, the mixed oil samples have the characteristics of source rocks of Huangshanjie Formation, Yangxia Formation and Kezilenur Formation. The Jurassic oil source rocks in the northern area of Yangxia Sag (well YT-1) include source rocks in the Huangshanjie Formation and coal measure source rocks in the Yangxia Formation and Kezilenur Formation, and the oil source conditions are more favorable.

### *4.3. Diagenetic evolution and densification of reservoir*

#### *4.3.1. Petrological characteristics*

For the Yangxia Formation and Ahe Formation in Yangxia Sag, braid delta plain front sand bodies are widely developed, which show discontinuous accretion in the vertical direction and lenticular lateral contact in the lateral direction, and constitute the main body of Jurassic tight oil and gas exploration and development (Wei GQ et al., 2021). According to the microscopic identification of the common thin section of the core, the main rock types of Yangxia Formation are mainly lithic sandstone and a minor amount are feldspar lithic sandstone (Fig. 7a). Among them, quartz content is between 23% and 67%, feldspar content is between 5% and 23%, and detrital cuttings content is between 38% and 62%, with metamorphic rock debris cuttings dominating. The interstitial material has an average content of between 5% and 12%, and is mostly composed of heterozygous material, which is typically 5% to 10%. The composition of the isthmus is primarily argillaceous. The rocks of the Ahe Formation in the Yangxia sag are all lithic sandstones, ranging from 23% to 58% quartz, 4% to 18% feldspar, and 40% to 65% conglomerate.

#### *4.3.2. Reservoir physical properties and pore types*

The reservoir of the Yangxia Formation has a porosity between 1.0% and 10.2%, with an average of 7.3%. The permeability is $0.3\times10^{-3}$ – $41.4\times10^{-3}$ μm$^2$, averaging as $1.0\times10^{-3}$ μm$^2$ (Fig. 7b). The porosity of the Ahe Formation ranges from 1.8% to 11.3%, with an average of 8.0%. The permeability is $0.003\times10^{-3}$ – $23.5\times10^{-3}$μm$^2$, with an average of $1.0\times10^{-3}$ μm$^2$ (Fig. 7c). There is an excellent positive correlation between the porosity and permeability of reservoir rocks in the Yangxia and Ahe Formation. Due to the development of micro-fractures, the permeability of the reservoir increases significantly, showing the characteristics of low porosity to medium high permeability (Fig. 7b). According to the distribution characteristics of reservoir porosity, Ahe Formation in Yangxia sag belongs to tight reservoir, but the permeability is allegedly higher than other tight reservoirs. Thin-cut observations of the casts show that the pore types of the Ahe Formation are mainly intergranular dissolved pores, intergranular dissolved pores and microfractures, while those of the Yangxia Formation are mostly intergranular dissolved pores, intergranular dissolved pores and microfractures (Fig. 8). There are both edge cracks along the grain and microcracks cutting through the grain (Fig. 8). Zhang RH et al., (2020) systematically studied the influence of tectonic extrusion on the diagnostic process of reservoir rocks, and concluded that the matrix porosity was drastically reduced, and the structural porosity was reduced by 8.8%/100 MPa. The permeability increases due to fracture formation, with increasing the permeability by a factor of 10–100. Increasing the formation fluid pressure value, an anomalous extreme pressure is formed. The dissociation along the fracture network system is enhanced by accelerating the intensity of the water-rock reaction, which favors the formation and development of localized cement (Zhang RH et al., 2020). The eastern Yangxia sag is adjacent to the Orogenic Zone and has undergone multi-stage tectonic movements. Many microfractures are generated in the reservoir, which is an essential reason for the considerably improved permeability of the tight reservoir.

#### *4.3.3. Diagenetic types and sequence of diagenetic evolution*

The primordial sedimentary conditions of the reservoir provide the material basis for the formation of the reservoir.

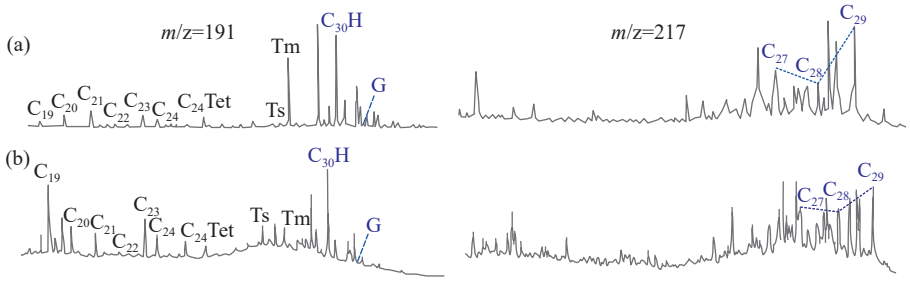


**Fig. 6.** Distribution characteristics of biomarker in crude oil of Yangxia Formation (a) and Ahe Formation (b) in Yangxia sag. Note: $C_{24}$Tet, $C_{24}$ tetracyclic terpanes; $C_{26}$ TT, $C_{26}$ tetracyclic terpanes; $C_{30}$H, $C_{30}$ hopanes; D, $C_{30}$ rearranged hopanes; G, gammacerane.

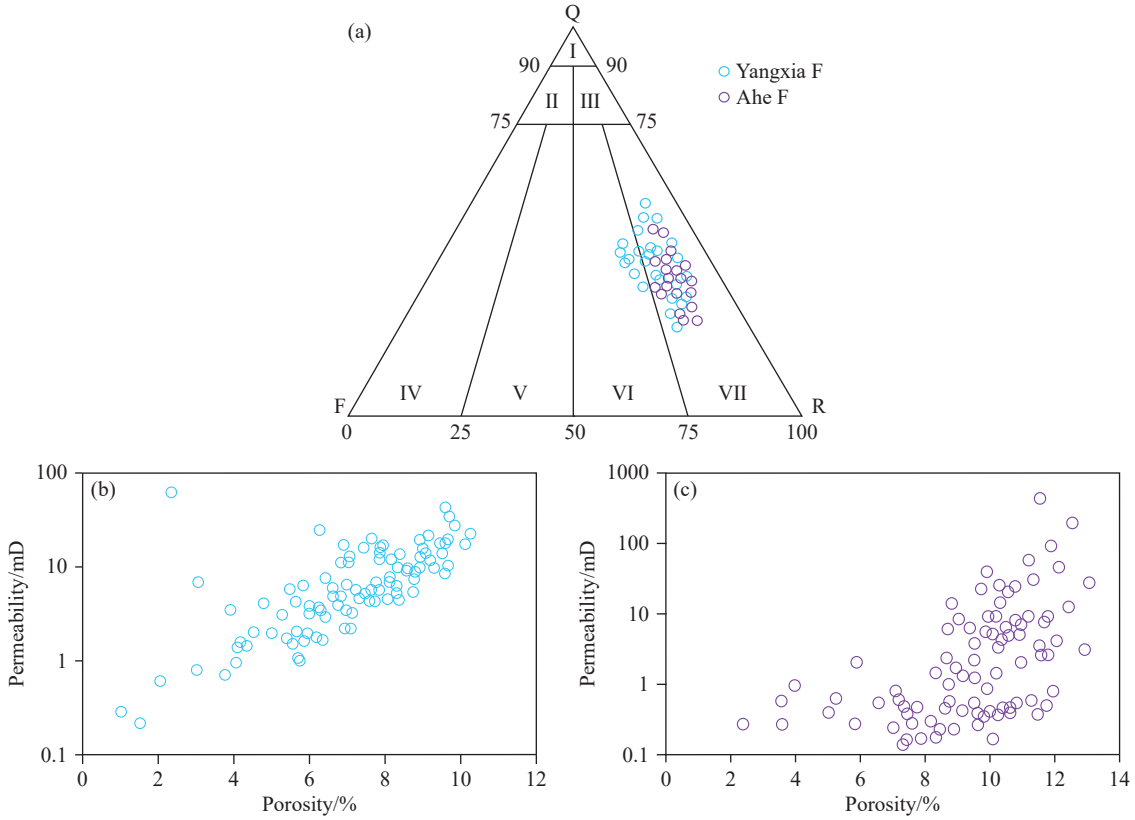


**Fig. 7.** Rock classification of sandstone reservoirs of Yangxia and Ahe Formations in Yangxia sag (a) and their porosity and permeability comparison (b and c). Ⅰ–Quartz sandstone; Ⅱ–feldspar quartz sandstone; Ⅲ–lithic quartz sandstone; Ⅳ–feldspar sandstone; Ⅴ–lithic feldspar sandstone; Ⅵ–feldspar lithic sandstone; Ⅶ–lithic sandstone.

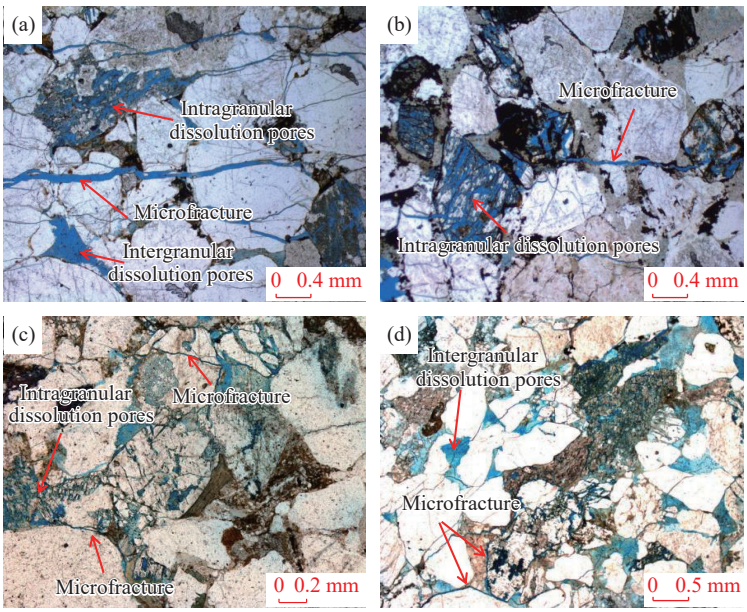


**Fig. 8.** Pore types of sandstone reservoirs of Jurassic Ahe Formation and Yangxia Formation in Yangxia sag. a–Well YT-1, 7787.64 m, $J_1a$, lithic sandstone. There are intergranular dissolved pores in the rock, and feldspar dissolution is relatively common, leading to the formation of intra - granular dissolved pores. There is less debris. The rock cracks are highly developed, cutting through particles intermittently, extending in parallel, and connecting with the pores. b–Well YT-1, 7791.60 m, $J_1a$, lithic sandstone. The pores are mainly grain - dissolved pores. Feldspar dissolution is more obvious, and dissolution occurs along the cleavage and cracks, forming sieve - like dissolved pores. Debris dissolution is less. Microcracks are parallel to the plane and are distributed intermittently. c–Well YX-2, 5295.87 m, $J_1y$, coarse-grained feldspar lithic sandstone. There are only a few intra - granular dissolution pores. Micro - cracks can be seen in feldspar and some lithic grains at the edges of a few particles. d–Well YX-2, 5304.90 m, $J_1y$. There are a small number of intergranular pores in coarse-grained lithic sandstone, solution pores in feldspar, micropores in argillaceous material, and a small number of grain margin fractures and microfractures extending through the particles.

After the evolution of the reservoir through geological burial and diagenesis, the present pore structure characteristics are the result of the joint transformation of different burial methods and multiple diagenesis (Liu MJ et al., 2017; Pan R et al., 2018). Burial and diagenetic influences in different geological periods control the evolutionary configuration of reservoir space. To conduct quantitative research on reservoir porosity evolution, it is necessary to combine the burial history and thermal history of strata to restore the temporal and spatial attributes of reservoir diagenesis process, to clarify the sequence of occurrence of major diagenesis and the influence of major diagenesis on reservoir pore formation and destruction (Pan R et al., 2018).

The reservoir burial process in the Yangxia Formation and the Ahe Formation can be divided into three stages, namely, the early slow-shallow burial stage, the late fast-deep burial stage, and the ultra-late adjusted uplift stage. The two sets of reservoirs have strong diagenesis, and the rock particles are in contact with concave-convex lines (Fig. 9a). In the early slow-shallow burial stage, the reservoir is in the low-temperature diagenetic evolution stage for a long time. At this time, the acidic fluid formed by the thermal evolution of the coal-measure source rocks of the Jurassic Yangxia Formation and Kezilenuer Formation resulted in an acidic fluid environment in the reservoirs, which to some extent inhibited the cementation of carbonates in the early period. It is generally believed that carbonate cements fill the pores, which reduces the original pores (Fig. 9b), but the hardness of carbonate plays a positive role in improving the compaction resistance of the reservoir. The formation of less carbonate cements in the early stage is an important factor that greatly reduces the porosity of the reservoir under the action of compaction during the rapid burial stage. In the late stage of rapid deep burial, there are not only vertical compaction stress of overlying sediments, but also compressive stress caused by tectonic activities. Vertical compaction and structural compaction are the reasons for the reduction of residual primary intergranular pores in the reservoir (Wang K et al., 2020). The characteristics of bending deformation of plastic minerals such as mica can be seen under the section. However, compared with other areas of Kuqa Depression, the Jurassic reservoir compaction in this study area is of moderate strength (Li GX et al., 2018). Meanwhile, under the influence of late tectonic movement, the reservoir fluid became more active, and the flexible materials such as feldspar and rock debris dissolved, forming secondary dissolution pores (Fig. 9c, d). Meanwhile, with the increase of temperature, the dissolution of carbonate minerals will be limited, mainly reflecting the precipitation process, and the dissolution effect is weak (Segnit ER, 1962; Cao YC et al., 2022). In the late adjustment uplift stage, the stress is released and the porosity recovers with some bounce. With the formation of acidic

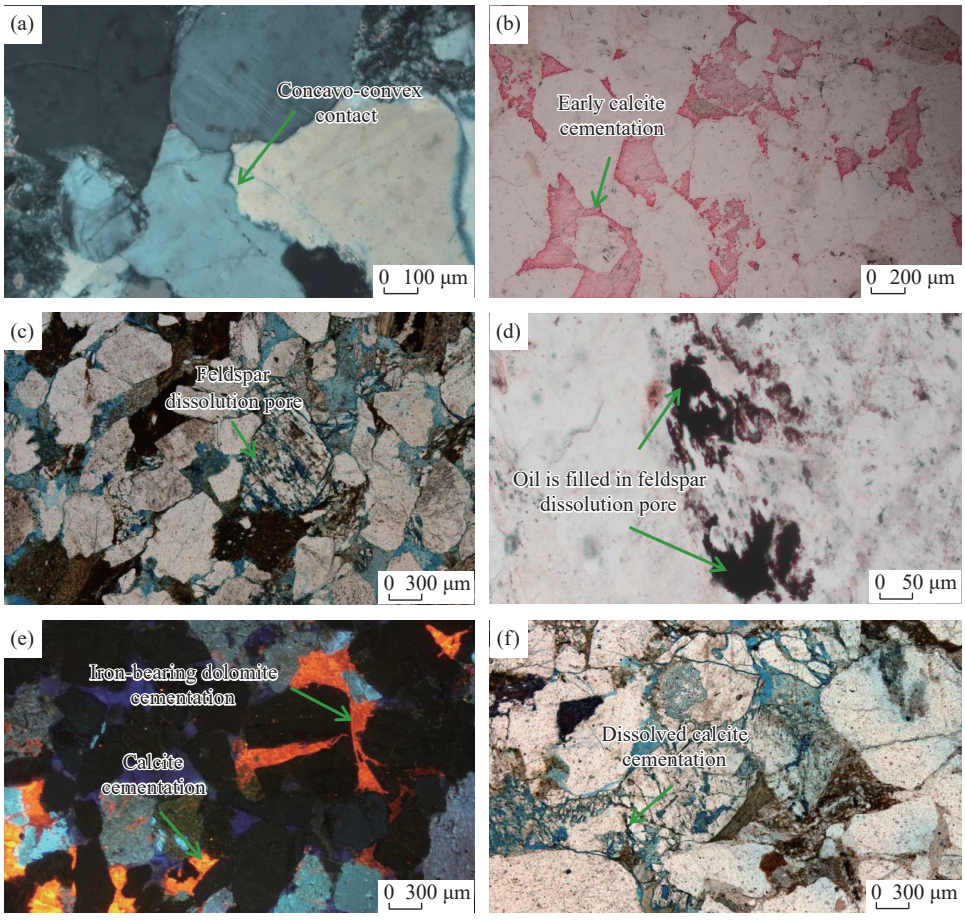


**Fig. 9.** Diagenetic characteristics of tight reservoirs in Ahe and Yangxia formations in Yangxia sag.

fluids from organic acids and $CO_2$ from the charging of oil and gas, the dissolution of calcite and ferrocalcite occurs again to form secondary pores, which also leads to the formation of fractures and micro-fractures.

The reservoirs of Ahe Formation and Yangxia Formation have similar diagenetic evolution process. Based on the observation of thin sections and the sedimentary and burial history of the reservoir, the contact relationship of mineral particles and the maturity of organic matter show that the Ahe Formation was in the early diagenetic stage A for a long time in the early burial period. While the early compaction was slow, the early calcite cementation reduced the porosity of the reservoir. Then there is the process of dissolution of the feldspar, resulting in the increase of pores, the precipitation and dissolution of calcite, iron-bearing calcite, or dolomite. Comprehensive analysis shows that the diagenetic evolution sequence of Ahe Formation reservoir is as follows: Compaction (slow shallow burial stage) → calcite cementation → compaction (fast deep burial stage) → feldspar dissolution → calcite and ferrocalcite cementation → calcite and ferrocalcite dissolution. The diagenetic evolution sequence of Yangxia Formation reservoir is as follows: Compaction (slow shallow burial stage) → secondary quartz enlargement → compaction (fast deep burial stage) → feldspar dissolution → calcite and iron-bearing dolomite cementation → calcite and iron-bearing dolomite dissolution. The diagenetic evolution process of tight reservoirs in Ahe Formation and Yangxia Formation is similar, and the differences are mainly reflected in the middle diagenetic stage. The former is characterized by the cementation and dissolution of calcite and ferrocalcite, while the latter is characterized by the cementation and dissolution of calcite and iron-bearing dolomite.

*4.3.4. Porosity evolution and recovery of tight reservoir*

The porosity evolution and recovery process of tight reservoir is the core issue of quantitative reservoir research, and the basis for studying the coupling relationship between reservoir densification and oil and gas charging. Many scholars have conducted in-depth research in this respect, and established a series of methods or relevant mathematical models for reservoir densification process restoration (Liu MJ et al., 2017; Zhao CJ et al., 2021). The basic principle of the recovery process for porosity evolution is to fully consider and characterize quantitatively the effects of mechanical compaction, dissolution, and cementation of new minerals on the physical properties of the reservoir at different stages of diagenetic evolution. For this, the commonly used methods include empirical formula method, porosity influence factor method, inversion stripping method, diagenetic effect simulation method (Dutton SP and Land LS, 1988; Wang K et al., 2020; Zhao CJ et al., 2021).

According to the diagenetic evolution sequence, the pore evolution of the Ahe Formation and Yangxia Formation can be roughly divided into four stages, that is, early cementation → dissolution → late cementation → dissolution, and compaction runs through the whole diagenetic process. In this study, diagenetic effect simulation method is adopted to recover the reservoir porosity evolution history with diagenetic evolution sequence as the constraint condition, including the recovery of primary porosity, the process of pore reduction caused by compaction, the process of pore reduction caused by cementation and the process of pore increase caused by dissolution.

(i) Primary porosity

The primary porosity is the beginning of the forward modeling of porosity. The primary porosity after sandstone deposition is mainly affected by particle sorting, and its recovery methods can be divided into two categories (Zhao CJ et al., 2021): (1) According to the modern sandy sediment porosity test (Atkins JE and Mcbride EF, 1992), the initial porosity is mostly 40%–45%. (2) A control chart or quantitative formula for the recovery of original porosity was established based on the laboratory artificial filling experiment of clastic particles (Beard PK and Weyl DC, 1973; Cao YC et al., 2011), which is most commonly used in the standard chart established by Beard et al. The empirical formula of original porosity ($\Phi_0$) is as follows (Equ. 1):

$$\varnothing_0 = 20.91 - 22.90/S_0 \quad (1)$$

Where $\Phi_0$ is the primary porosity of sandstone, %; $S_0$ is Trask sorting coefficient (Equ. 2)

$$S_0 = \sqrt{P_{25}/P_{75}} \quad (2)$$

Where $P_{25}$ is the particle size at 25% of the particle size accumulation curve, μm; $P_{75}$ is the particle size at 75% of the particle size accumulation curve, μm.

(ii) Porosity reduced by cementation and increased by dissolution

The authigenic mineral cementation during diagenesis is the key to the physical property's reduction of reservoirs. Authigenic minerals include multi-stage carbonate cements, siliceous cements and authigenic clay mineral cements. The quantitative analysis of the cement at different stages is mainly based on the available thin-section analysis data to determine the cement content formed at each diagenetic stage. In general, the secondary pores formed by dissolution are mainly dissolved pores in feldspar grains and intercrystalline pores. Therefore, the quantitative analysis to simulate the increase of porosity caused by dissolution is mainly to calculate the contribution of dissolved pores in grains and intercrystalline pores. The early cementation mainly includes the secondary increase of calcite and quartz, and the decrease of porosity is equal to the pores occupied by these two cements, which are respectively $\upsilon_1$ and $\upsilon_2$. The increment of porosity caused by dissolution is the sum of the pores occupied by intergranular dissolved pores and ingranular dissolved pores, which is $\varnothing_1$. The late stage was mainly due to ferrocalcite cementation and tectonic fracture formation, which accounted for porosity of $\upsilon_3$ and $\varnothing_2$. The reduction in porosity caused by compaction, $\varnothing_3$, is equal to the original

porosity minus the change in porosity caused by the above parameters, namely (Equ. 3):

$$\varnothing_3 = \varnothing_0 - (\upsilon_1 + \upsilon_2 + \upsilon_3) + \varnothing_1 + \varnothing_2 - \varnothing_{now} \quad (3)$$

Based on the computer image analysis of the cast thin sections, it is possible to calculate the surface porosity occupied by the different minerals, which needs to be translated into porosity. Therefore, in a quantitative calculation of the effect of diagenesis on porosity, a functional relationship between the surface porosity and the porosity transition should be established. According to the comparison between the surface porosity of various diagenetic influences and the measured porosity calculated by ImageJ and Photoshop software, the conversion function of surface porosity and measured porosity can be fitted (Fig. 10; Equ. 4):

$$y = 0.9287\ln(x) + 7.178, R^2 = 0.7042 \quad (4)$$

Where, $y$ is porosity, $x$ is surface porosity, and $R$ is correlation coefficient.

(iii) Porosity reduced by compaction

Compaction runs through the whole process of diagenesis in the study area. It is very important to correctly recover the porosity reduction caused by compaction in each geological period. Previous studies have shown that under normal compaction conditions, the porosity varies exponentially with the burial depth. Considering the influence of burial time on compaction, predecessors divide burial stages based on the burial history, multiply the depth of settlement at each stage with the time experienced, and the ratio of the product to the sum of the products can be taken as the percentage of the porosity reduced by compaction at each stage in the total porosity reduced (Liu Z et al., 2007). In the meantime, the burial factor (α) was introduced to correct the effect of the change in compaction efficiency caused by the increase of burial depth on the porosity reduction in compaction (Pan R et al., 2018). The reduction of the pore caused by compaction during settlement are (Equs. 5, 6):

$$\varnothing_{2i} = \varnothing_2 \times C_i \quad (5)$$

$$C_i = \frac{\Delta H_i \times \Delta T_i a}{\sum_{i=1}^{n} \Delta H_i \times \Delta T_i a} \quad (6)$$

Where, $\Phi_{2i}$ is the amount of porosity reduced by compaction in the $i$ th settlement; $C_i$ is the proportion of porosity reduced; $\Delta H_i$ is the depth of the $i$ th settlement; $\Delta T_i$ is the time of the $i$ th settlement; α is the burial factor ($\alpha=2^n$; Early burial stage, $n$=0; Medium burial stage, $n$=1; Late burial stage, $n$=2).

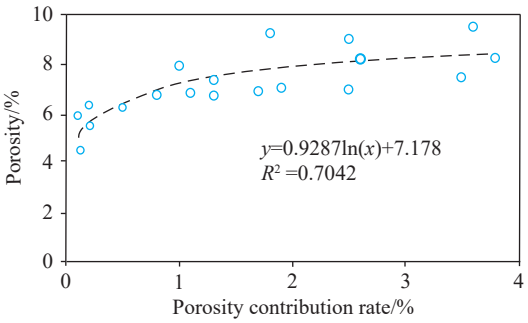


**Fig. 10.** Fitting curve of porosity and surface porosity.

(iv) Results of the recovery of porosity evolution

The influence of diagenesis on the porosity of the reservoir at different epochs can be obtained by the method described above. Combined with the burial history of the formation, the influence values can be assigned to each geological historical period, and eventually the evolution history of the porosity of the sandstone reservoir can be recovered. In the case of the 7709.34 m lithic sandstone sample from the well YT-1, the measured porosity is 8.2%. According to Equation 1-1, the original porosity of the sample is 34.0%. The contribution of diagenesis to porosity can be converted based on the values of the influence of various diagenesis on the surface porosity calculated by image analysis software, and combined with the burial history to calculate the influence of diagenesis over various geological historical periods. According to the burial history, the Ahe Formation of well YT-1 has experienced five settlements (Fig. 12). The pore reduction ratio and amount of porosity caused by compaction in each settlement period are calculated according to Equation 1–5 and 1–6, among which the total pore reduction by compaction is 24.6% (Table 1, Table 2).

In summary, the effect of diagenesis on the reservoir porosity is matched to each stage of reservoir diagenesis and then the evolution of the reservoir porosity is recovered. In 201.3 Ma, the Ahe Formation began to receive deposits, and the original porosity of the reservoir was 34.0%. At 163.0 Ma, the depth of the formation was 958 m. The first settlement

**Table 1. Pore reduction caused by compaction of 7709.34 m lithic sandstone samples from well YT-1 at different stages.**

| Stage of settlement | Duration of settlement /Ma | Depth of settlement /m | burial factor α | Pore reduction ratio $C_i$ | Reduction of pores by compaction /% |
|---|---|---|---|---|---|
| 1 | 46.8 | 958 | 1 | 0.15 | 4.1 |
| 2 | 37.0 | 428 | 1 | 0.04 | 1.1 |
| 3 | 31.5 | 172.4 | 2 | 0.08 | 2.0 |
| 4 | 20.6 | 4844 | 2 | 0.70 | 12.3 |
| 5 | 2.0 | 1336 | 4 | 0.03 | 5.1 |

**Table 2. Influence of diagenesis on porosity of 7709.34 m lithic sandstone samples from well YT-1 in different geological periods.**

| Time/Ma | Ancient buried depth /m | Diagenesis | Surface porosity /% | Porosity of conversion /% |
|---|---|---|---|---|
| 201.3–5.2 | 0–4575 | Cementation (early stage) | 2.6 | 5.9 |
| 5.2–3.8 | 4400–5815 | Dissolution and tectonic fractures | 1.5 | 3.2 |
| 3.8–2.8 | 5815–6638 | Cementation (late stage) | 0.2 | 1.0 |
| 2.8–2.3 | 6638–7050 | Dissolution and tectonic fractures | 1.4 | 3.0 |

ended and authentically chlorite film developed. The porosity decreased by 4.1% due to compaction, and the porosity was 29.9% at this time. Between 163.0 Ma and 5.2 Ma, the Ahe Formation experienced the second, third and fourth subsidence respectively, during which quartz secondary enlargement and calcite cementation occurred. The porosity decreased by 5.9% due to cementation, and 15.4% due to compaction. At this time, the reservoir paleo-porosity was 8.6%. From 5.2 Ma to 2.3 Ma, Ahe Formation experienced the fifth subsidence, during which the source rocks matured rapidly and generated organic acids. The dissolution resulted in the increase of pores, and the calcite cementation and iron calcite cementation occurred. Overall, the increase in porosity due to dissolution was 6.2%, while the decrease due to compaction was 5.1%. Cementation reduced the pores by 1.0%, and the paleoporosity of the reservoir was 8.7%. The physical properties of the reservoir have changed little since 2.3 Ma. The result of paleoporosity restoration is about 8.7%, and the average measured porosity is 8.2%. The evolution results are basically consistent with the measured data. Within the allowed error range, it indicates that the porosity restoration results are reliable, that is, the Ahe Formation reservoir began to densification at about 6.0 Ma. Similarly, the lithic sandstone samples from the Yangxia Formation at 5304.4 m in Well YX-2 were selected to carry out the porosity recovery. The measured porosity is 6.1% and the paleo porosity recovery result is about 6.0%, indicating that the recovery results are reliable. Therefore, Yangxia Formation reservoir began to densify at about 3.5 Ma. The porosity of the Jurassic reservoir in the Yangxia sag experienced a process of rapid decrease, slow increase, and slow decrease again. Compaction and pressure-solubilization are the direct causes of most of the primary intergranular pore losses, which have a clearly destructive effect on the reservoir. The cementation of carbonate minerals and the secondary increase of quartz damage the reservoir to varying degrees. Fracture and dissolution of organic acids improve the physical properties of the reservoir to a certain extent, especially the formation of microfractures, which is important for improving the permeability of the reservoir. Reservoir physical properties recovery is a semi-quantized numerical simulation technique that can obtain the evolution of the physical properties of the reservoir and determine the time of densification. This time it is not accurate enough and there are still some errors.

## 5. Discussion

### *5.1. Characteristics of the hydrocarbon accumulation process*

#### *5.1.1. Hydrocarbon accumulation period*

Based on the samples from wells YX-2 and YT-1, the appropriate hydrocarbon inclusions were selected to determine the homogenization temperature of the associated saline inclusions, and then the hydrocarbon accumulation period was determined based on the burial history and thermal history. Within the studied area, the oil and gas inclusions in the Yangxia and Ahe formations occur mainly in quartz grains and secondary enlarged margins, and can develop two phases of inclusions. Among them, the inclusion of the first phase is mainly characterized by oil, and orange (Fig. 11a) and yellow fluorescence (Fig. 11d) can be seen, reflecting the early oil charging process. The second phase consists of bluish-white fluorescent hydrocarbon inclusions (Figs. 11b, e) and non-fluorescent hydrocarbon inclusions (Figs. 11c, f), reflecting hydrocarbon or gas charging with higher maturity. The homogenization temperature was measured for salt water

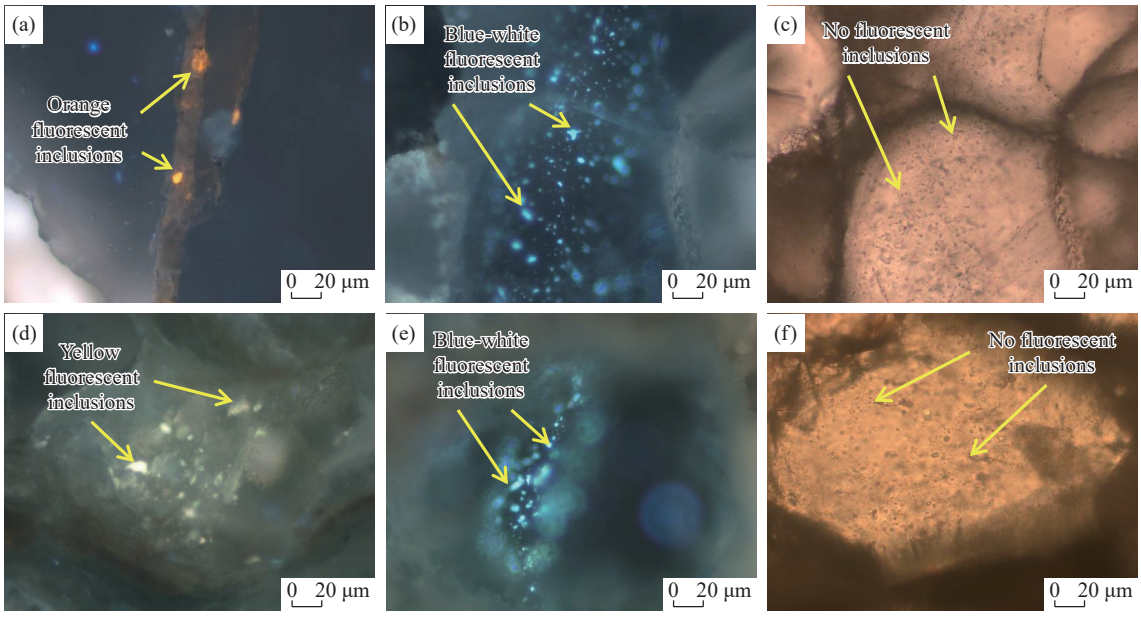


**Fig. 11.** Photomicrographs of representative inclusions under transmitted and UV light observed. (a), (b) and (c), inclusion characteristics of Ahe Formation in Well YT-1; a–oil inclusions with yellow fluorescence colour; b–oil inclusions with blue-white fluorescence colour; c–gaseous inclusion, no fluorescence. (d), (e) and (f), inclusion characteristics of Yangxia Formation in Well YX-2; d–oil inclusions with yellow fluorescence colour; e–oil inclusions with blue-white fluorescence colour; f–gaseous inclusion, no fluorescence.

inclusions associated with oil and gas inclusions in both phases.

Oil-bearing inclusions can also be found in the Ahe Formation reservoir of well YT-1. The fluorescence color is orange and blue-white (Figs. 11a, b), capturing the low-maturity to mature oil generated from the source rock, and the peak homogenization temperature of the associated brine inclusions ranges from 110°C to 125°C. The peak homogenization temperature of natural gas inclusions associated with brine inclusions ranges from 130°C to 145°C. Combined with the burial thermal history analysis of well YT-1, it can be concluded that the charging time of oil and natural gas in Ahe Formation is between 4.8–3.5 Ma, and between 2.8Ma and 1.7 Ma (Fig. 12). The fluorescence display of hydrocarbon inclusions in the Yangxia Formation of well YX-2 is yellowish and bluish-white (Figs. 11d, e), indicating that low-maturity to mature was captured, and the peak homogenization temperature of its associated brine inclusions ranges from 110°C to 120°C. The peak homogenization temperature of natural gas associated brine inclusions ranges from 130°C to 145°C, which is higher than that of crude oil associated inclusions (Fig. 12). Combined with the burial and thermal history of well YX-2, the Yangxia Formation experienced two periods of oil and gas charging, with the early crude oil charging period ranging from 4.8–4.2 Ma and the late natural gas charging period ranging from 3.7–2.8 Ma (Fig. 13). Therefore, there are two phases of early oil and late gas accumulating in the reservoirs of the Jurassic Ahe Formation and Yangxia Formation in the eastern Yangxia sag.

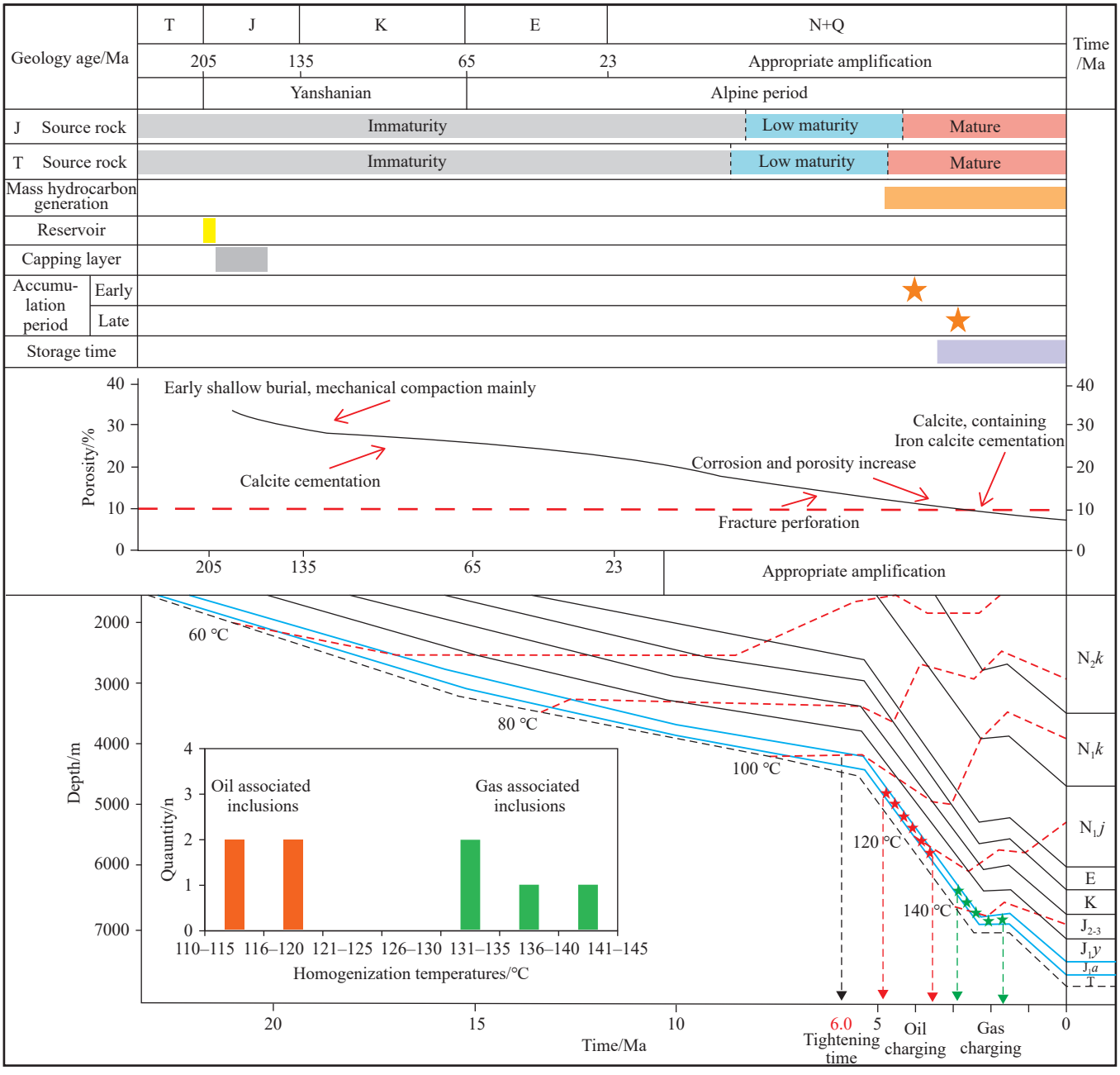


**Fig. 12.** Characteristics of dynamic accumulation process in Well YT-1.

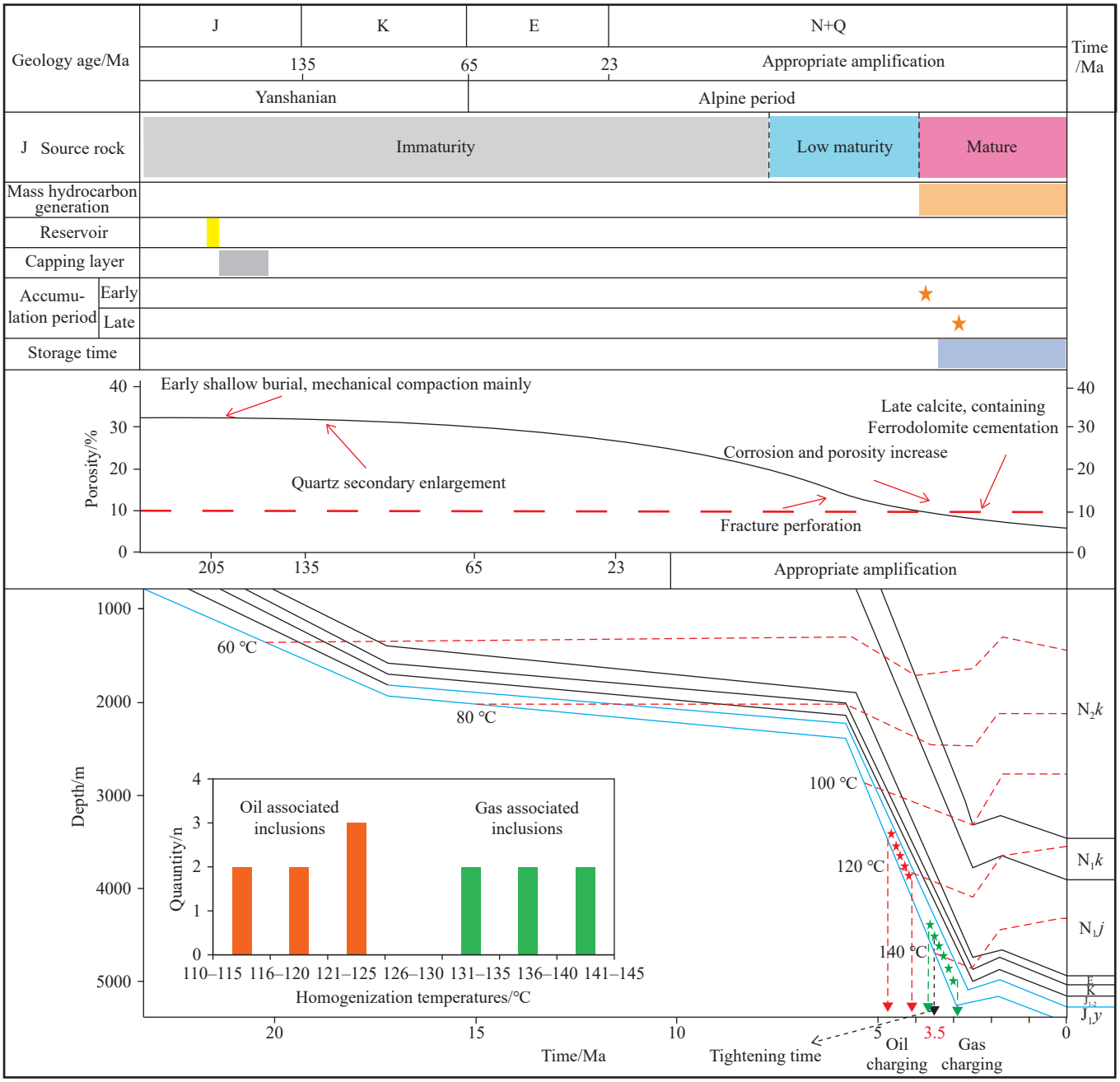


**Fig. 13.** Characteristics of dynamic accumulation process in Well YX-2.

*5.1.2. Hydrocarbon accumulation process*

The process of dynamic hydrocarbon accumulation is affected by several factors, the most critical of which are the structural properties of the source and reservoir and the temporal relationship between the reservoir densification and the hydrocarbon charging period. There are two types of source and reservoir structures for Triassic and Jurassic tight gas in the eastern part of the Yangxia sag. In the northern part of the depression, the source rock of Triassic Huangshanjie Formation proved to be oil-supplying, forming a relationship of lower generation and upper reservoir structure with Ahe Formation and Yangxia Formation reservoirs. The tight oil of Yangxia Formation can be supplied by coal measure source rocks from Jurassic Yangxia Formation and Kezilenuer Formation. Therefore, the internal structure of the Yangxia Formation has the characteristics of "self-generating and self-storing".

This paper analyzes the hydrocarbon accumulation process of Ahe Formation by taking well YT-1 as an example. This well is in the northeastern part of Yangxia sag (Fig. 1c). The simulation analysis of the thermal evolution history of well YT-1 and well YX-2 shows that the burial depth in Yangxia sag has increased rapidly since the Neogene, while the overall burial depth before the Neogene has a small change range, which is consistent with the characteristics of early shallow burial and late deep burial. With vitrinite reflectance ($R_o$) of 0.7% as the oil generation threshold, the Triassic source rocks in the northern Yangxia sag began to mature after 6.5 Ma (Fig. 12). The Jurassic source rocks began to mature at 5.5 Ma and entered the oil-generation

window slightly later than that of Triassic (Fig. 12). In contrast, only Jurassic source rocks are developed in the southern part of Yangxia sag, and the maturity time of source rocks is later than that in the northern part, with oil generation starting about 3.6 Ma (Fig. 13).

After deposition, the Ahe Formation sandstone underwent a long period of shallow and slow burial, and the reservoir began to densify around 6.0 Ma ago. Oil and gas in Ahe Formation of well YT-1 are mainly derived from the source rocks of the Huangshanjie Formation, which began to mature after 6.5 Ma ago, close to the time of reservoir densification, and the oil with low maturity generated in the early stage migrated vertically to the Ahe Formation reservoirs (Fig. 12). Subsequently, in the process of rapid formation depth burial, the maturity of the source rock increases continuously. At this time, the reservoir has been densified, and oil with higher maturity enters the tight reservoir under the action of hydrocarbon generation pressure. During the gas charging period of the Ahe Formation, the Triassic source rocks did not reach a large amount of gas generation stage, and the natural gas should mainly come from the source rocks of Huangshanjie Formation. Taking well YX-2 as an example to analyze the hydrocarbon accumulation process of Yangxia Formation, the oil and gas mainly come from the Jurassic coal measure source rocks, because the local source rocks have not reached many gasses generation stage, only can provide a small amount of oil, natural gas is mainly from the Jurassic coal measure source rocks in Yangxia sag. In the early charging period of Yangxia Formation, the reservoir was not densified (about 3.5 Ma), and the oil could be accumulated under the action of buoyancy. During the gas charging period, the densification process of Yangxia Formation was basically synchronized, and the oil and gas generated from the local Jurassic source rock entered the tight reservoir under the pressure of hydrocarbon generation (Fig. 13).

### *5.2. Tight oil and gas exploration potential*

#### *5.2.1. Hydrocarbon generation potential evaluation*

The hydrocarbon generation potential of the source rock is a prerequisite for controlling the build-up of oil and gas. The northern structure represented by well YT-1 and the southern structure area represented by well YX-2 have moderate maturity of local source rocks, which can generate a certain amount of oil and gas. According to the results of the Jurassic source correlation, the lacustrine source rocks of the Huangshanjie Formation of the Triassic period and the coal-measure source rocks of the Yangxia and Kizilenur formations in the study area all contributed. However, from the planar distribution of the source rocks of the different formations, that the Triassic source rocks have a limited distribution in the region studied, and that it should be dominated by the Jurassic Coal Measures. Based on the available source rock data, the $R_o$ values for the Jurassic source rocks range from 0.98% to 1.15%, reflecting that the source rocks are primarily in the mature evolutionary stage. According to the geochemical evaluation of the source rocks described above, Jurassic source rocks with high organic matter abundances developed in the eastern Yangxia sag, and all within the effective hydrocarbon burial depth range can be used as effective oil and gas source rocks. Based on the thickness distribution of the source rock, the organic geochemical properties and the blood flow of the depression, the hydrocarbon production strength of the Jurassic source rock was evaluated with the help of basin simulation techniques. The gas intensity of Jurassic source rocks in the eastern Yangxia sag is mainly $5\times10^9$ – $10\times10^9$ $m^3/km^2$, which gradually decreases from northwest to southeast (Fig. 14). Wei GQ et al., (2013) and Li J et al., (2013) proposed through a lot of exploration practice that large tight sandstone gas fields can be formed in areas with gas intensity greater than $1\times10^9$ $m^3/km^2$, but the accumulation process in areas with low hydrocarbon generation intensity is complicated. The

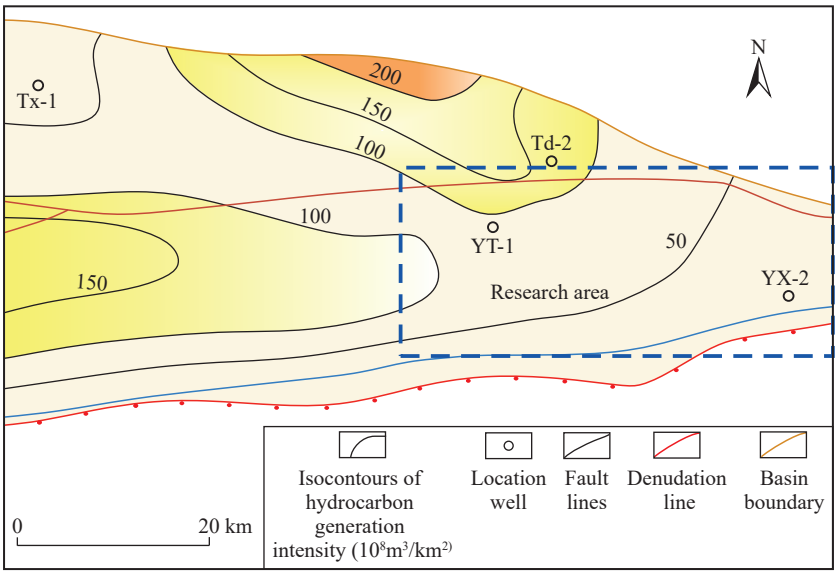


**Fig. 14.** Plane distribution of gas intensity of Jurassic source rocks in Eastern Yangxia Sag.

natural gas is enriched in high parts of sand bodies with good reservoir physical properties, and the overall gas saturation of sand bodies with relatively poor physical properties is low. What' more, Yangxia sag includes one of the two hydrocarbon generating centers in the Kuqa Depression. The maximum burial depth is over 8000 m, the present formation temperature is over 200°C, and the source rocks have reached the high-superheated evolution stage and are in the stage of abundant gas generation (Wei GQ et al., 2021; Zhi FQ et al., 2023). The migration channel of natural gas can be the regional unconformity between Jurassic and Triassic (Liu C et al., 2021; Fan S et al., 2022).

*5.2.2. Tight oil and gas accumulation potential*

The densification of reservoirs is another key factor for Jurassic hydrocarbon accumulation in Eastern Yangxia sag. Due to structural compression, many micro-fractures developed in the reservoir in the study area, which significantly improved the permeability of the reservoir and formed a fracture network system. Microfractures can communicate with isolated micropores to form relatively connected reservoir spaces, which reduces the charging resistance of the gas to some extent. This is a favorable condition for gas charging in the Jurassic tight reservoir of Yangxia sag compared to tight sandstone reservoirs elsewhere in the world. In addition, for late gas migration, Luo XR et al., (2010) believed that the early oil charging in the reservoir inhibited the influence of fibrous illite and reduced the damage to reservoir permeability. The migration path of the early oil charging then becomes the migration path of late gas, reducing the resistance of gas charging and improving the efficiency of gas charging in tight reservoirs. Therefore, the natural gas can migrate to the structural area through the transport system such as faults and connected sand bodies, and enter the tight reservoir pores along the charging channels that previously preserved oil under the communication of micro-fractures, forming tight sandstone gas reservoirs.

As a result, the gas intensity of the Jurassic source rocks in the northern part of the study area is high, the accumulation conditions of the dense sandstone bodies in the high parts of the Yangxia and Ahe formations or in the slopes are good, and the potential for continuous tight sandstone reservoirs is great. In the southern region, the gas intensity is low and the local source rock supply is significantly insufficient. The gas supply is mainly dependent on the high-quality source rock in the depression region, and the gas accumulates in higher parts of the structure through lateral migration. Since the gas charging period is slightly later than the reservoir identification period, this limits the gas accumulation efficiency of the tight reservoirs in the Yangxia and Ahe formations, and the high-grade portion of the structure may have better exploration potential. Therefore, the eastern portion of the Yangxia sag, where the sagging oriented tight sandstone oil and gas accumulations are better located than the southeastern margin can be used as a favorable area for Jurassic tight sandstone oil and gas exploration.

## 6. Conclusions

(i) The source rocks of Triassic Huangshanjie Formation in Yangxia Sag are mainly oil-generating, the source rocks of Jurassic Yangxia Formation are mainly gas-generating. Main source rocks include lacustrine source rocks of Huangshanjie Formation and coal measure source rocks of Yangxia Formation and Kezilenur Formation.

(ii) Jurassic Yangxia Formation and Ahe Formation are tight sandstone reservoir, which experienced two stages of early long-term shallow burial and late rapid deep burial, and Ahe Formation and Yangxia Formation reservoirs were densified at 6.5 Ma and 3.5 Ma respectively. The period is later than the reservoir densification time for Ahe Formation oil and gas, and Yangxia Formation oil was charged before the reservoir densified, and the late gas was charged after the reservoir densified.

(iii) The Jurassic source rocks in the eastern Yangxia sag are developed, and the hydrocarbon generation intensity has reached the basic conditions for the formation of tight sandstone gas reservoirs. Controlled by the difference in the distribution of the source rocks, the tight sandstone oil and gas accumulations in the direction of the depression are better than those on the southeastern margin, which can be used as a favorable area for Jurassic tight sandstone oil and gas exploration.

## CRediT authorship contribution statement

Cai-yuan Dong and Liang Zhang, conceived of the presented idea and developed the theory. Wei Yang and Zhen-ping Xu, carried out the experiment. Jun Li and Wei-dong Miao verified the analytical methods. All authors discussed the results and contributed to the final manuscript.

## Declaration of competing interest

The authors declare no conflicts of interest. This study is financially supported CNPC Scientific Research and Technology Development Project (No. 2023ZZ14YJ02).

## Acknowledgments

This study is financially supported by Joint Fund Project of National Natural Science Foundation (No. U22B6002) and CNPC Scientific Research and Technology Development Project (No. 2023ZZ14YJ02).

## References

Atkins JE, McBride EF. 1992. Porosity and Packing of Holocene River, Dune, and Beach Sands (1). AAPG Bulletin, 76(3), 339–355. doi: 10.1306/BDFF87F4-1718-11D7-8645000102C1865D.

Beard PK, Weyl DC. 1973. Influence of Texture on Porosity and Permeability of Unconsolidated Sand. AAPG Bulletin, 57(2), 349–369. doi: 10.1306/819A4272-16C5-11D7-8645000102C1865D.

Cao YC, Xi KL, Wang J, Yuan GH, Yang T. 2011. Preliminary Discussion of Simulation Experiments on the Mechanical Compaction and Physical Property Evolution of Sandstones.

Geoscience, 25(6), 1152–1158

Cao YC, Yuan GH, Wang YZ, Zan NM, Jin ZH, Liu KY, Xi KL, Wei YH, Sun PP. 2022. Successive formation of secondary pores *via* feldspar dissolution in deeply buried feldspar-rich clastic reservoirs in typical petroliferous basins and its petroleum geological significance. Science China Earth Sciences, 65(9), 1673–1703. doi: 10.1007/s11430-020-9931-9.

Chen JP, Huang DF. 1997. Hydrocarbon generation potential of mineral-bituminous matrix in source rocks. Geochimica, 26(6), 18–24 (in Chinese with English abstract). doi: 10.19700/j.0379-1726.1997.06.003.

Dai JX, Ni YY, Wu XQ. 2012. Tight gas in China and its significance in exploration and exploitation. Petroleum Exploration and Development, 39(3), 257–264 (in Chinese with English abstract).

Du SH, Zhao YP, Sun FQ, Shi YM. 2023. Estimations of the upper and lower depth limits for kerogen to generate oil/gas worldwide: A hypothesis. International Journal of Hydrogen Energy, 48(34), 12661–12671. doi: 10.1016/j.ijhydene.2022.12.125.

Dutta S, Greenwood PF, Brocke R, Schaefer RG, Mann U. 2006. New insights into the relationship between Tasmanites and tricyclic terpenoids. Organic Geochemistry, 37(1), 117–127. doi: 10.1016/j.orggeochem.2005.08.010.

Dutton SP, Land LS. 1988. Cementation and burial history of a low-permeability quartzarenite, Lower Cretaceous Travis Peak Formation, East Texas. Gsa Bulletin, 100(8), 1271–1282. doi: 10.1130/0016-7606(1988)100<1271:CABHOA>2.3.CO;2.

Fan S, Lu YH, Li L, Wei H, Zhang HF, Shen L. 2022. Geochemical characteristics, distribution and petroleum geological significance of Triassic-Jurassic source rocks in the Tugeerming and surrounding areas of Kuqa Depression, Tarim Basin. Natural Gas Geoscience, 33(12), 2074–2086 (in Chinese with English abstract).

Feng JW, Zhao, LB Wang YD, 2020. Controlling factors for productivity of ultra-deep tight reservoirs in Keshen gas field, Kuqa Depression. Acta Petrolei Sinica 41 (4), 78–88 (in Chinese with English abstract). doi: CNKI:SUN:SYXB.0.2020-04-012.

Guo XB, Huang ZL, Zhao LB, Han W, Ding C, Sun XW, Yan RT, Zhang TH, Yang XJ, Wang RM. 2019. Pore structure and multi-fractal analysis of tight sandstone using MIP, NMR and NMRC methods: A case study from the Kuqa depression, China. Journal of Petroleum Science and Engineering, 178, 544–558. doi: 10.1016/j.petrol.2019.03.069.

Guo XB, Zhao LB, Han W, Zhou LF, Huang ZL, Sun XW, Yang XJ, Zhang TH, Zhang CL. 2022. Geochemistry of formation water and implications for ultradeep tight sandstone of DK gas field in kuqa depression. Geofluids, 2022, 6514733. doi: 10.1155/2022/6514733.

Guo XW, Liu KY, Song Y, Zhao MJ, Liu SB, Zhuo QG, Lu XS. 2016. Influences of hydrocarbon charging and overpressure on reservoir porosity in Kela-2 gas field of the Kuqa Depression, Tarim Basin. Oil & Gas Geology, 37(6), 935–943 (in Chinese with English abstract). doi: 10.11743/ogg20160615.

Hao F, Zhou XH, Zou HY, Teng CY, Yang YY. 2012. Petroleum Charging and Leakage in the BZ25-1 Field, Bohai Bay Basin. Journal of Earth Science, 23(03), 253–267 doi: 10.1007/s12583-012-0251-8.

Huang DF, Li JC. 1982. X-diagram of Kerogen classification and the characters of Kerogen of standard humic type. Geochimica, (01), 21–30 (in Chinese with English abstract). doi: 10.1016/0013-7952(82)90005-9.

Jarvie DM. 2012. Shale resource systems for oil and gas: Part I–shale-gas resource systems. In: Breyer JA, (Ed. ), Shale Reservoirs–Giant Resources for the 21st Century. 97. AAPG Memoir, 69–87. doi: 10.1306/13321446M973489.

Jia AL, Wei YS, Guo Z, Wang GT, Meng DW, Huang SQ. 2022. Development status and prospect of tight sandstone gas in China. Natural Gas Industry, 42(1), 83–92 (in Chinese with English abstract). doi: 10.1016/J.NGIB.2022.10.001.

Jia D, Lu HF, Cai DS, Chen CM. 1997. Structural analyses of Kuqa foreland fold-thrust belt along the northern margin of Tarim Basin. Geotectonica et Metallogenia, (01), 1–8 (in Chinese with English abstract). doi:CNKI:SUN:DGYK.0.1997-01-000.

Jiang L, Zhang M. 2015. Geochemical Characteristics and Significances of Rearranged Hopanes in Hydrocarbon Source Rocks, Songliao Basin, NE China. Journal of Petroleum Science and Engineering, 131, 138–149. doi: 10.1016/j.petrol.2015.04.035.

Kruge MA, Mastalerz M, Solecki A, Stankiewicz BA. 1996. Organic geochemistry and petrology of oil source rocks, Carpathian Overthrust region, southeastern Poland-Implications for petroleum generation. Org Geochem, 24(8/9), 897–912. doi: 10.1016/S0146-6380(96)00067-8.

Law BE. 2002. Basin-centered gas systems. AAPG Bulletin, 86(11), 1891–1919. doi: 10.1306/61EEDDB4-173E-11D7-8645000102C1865D.

Li J, Wei GQ, Xie ZY. 2013. Accumulation mechanism and main controlling factors of large tight sandstone gas fields in China: Cases study on Ordos Basin and Sichuan Basin. Acta Petrolei Sinica, 34(S1), 14–28 (in Chinese with English abstract). doi: 10.7623/syxb2013S1002.

Li F, Jiang ZX, LI Z, Xiao ZY, Yuan WF, Cao SF. 2015. Characteristics of Condensate Oil and Its Significance for Hydrocarbon Accumulation in the Eastern Kuqa Depression. Geoscience, 29(6), 1425–1434

Li GX, Yi SW, Lin SG, Gao Y, Li MP, Li DJ, Wang CY. 2018. Reservoir characteristics and major factors influencing the reservoir quality of Lower Jurassic in eastern Kuqa Depression, Tarim Basin. Natural Gas Geoscience, 29(10), 1506–1517 doi: 10.11764/j.issn.1672-1926.2018.09.015.

Liu MJ, Liu Z, Wu YW, 2017. Differences in formation process of tight sandstone gas reservoirs in different substructures in Changling Fault Depression, Songliao Basin, NE China. Petroleum Exploration and Development, 44(2), 235–242 (in Chinese with English abstract). doi: 10.11698/PED.2017.02.07.

Liu Z, Shao XJ, Jin B, Li HY, Xu XM, Liang QS. 2007. Co-effect of depth and burial time on the evolution of porosity for classic rocks during the stage of compaction. Geoscience, (01), 125–132 (in Chinese with English abstract). doi: 10.1016/S1872-5813(07)60034-6.

Liu C, Chen SJ, Zhao JL. 2021. Hydrocarbon transportation system and accumulation simulation of Mesozoic-Cenozoic in south slope of Kuqa foreland basin. Natural Gas Geoscience, 32(10), 1450–1462 (in Chinese with English abstract). doi: 10.11764/j.issn.1672-1926.2021.04.008.

Liu JL, Jiang ZX, Liu KY, Gui LL, Xing JY, 2016. Hydrocarbon sources and charge history in the Southern Slope Region, Kuqa Foreland Basin, northwestern China. Marine & Petroleum Geology, 74, 26–46. doi: 10.1016/j.marpetgeo.2016.04.004.

Lu YH, Qian L, Lu XS, Yu HZ, Zhang K, Zhao Q. 2015. Geological conditions and resource potential of the tight gas reservoirs in Dibet area. Petroleum geology and oilfield development in daping, 34(4), 8–14 doi: 10.3969/J.ISSN.1000-3754.2015.04.002.

Luo XR, Zhang LP, Yang H. 2010. Oil accumulation oil process in the low-perme ability Chang-8$^{1}$ member of Longdong area the Ordos Basin. Oil & Gas Geology, 31(06), 770–778,837 (in Chinese with English abstract). doi: CNKI:SUN:SYYT.0.2010-06-013.

Moldowan JM, Fago FJ, Carlson RMK, Young DC, Duvne GA, Clardy J, Schoell M, Pillinger CT, Watt DS. 1991. Rearranged hopanes in sediments and petroleum. Geochimica et Cosmochimica Acta, 55(11), 3333–3353. doi: 10.1016/0016-7037(91)90492-N.

Ni LT, Zhong JH, Wang GL, Sun NL, Liu X, Hao B, Sun YK, Wang JS, Yang B, Qu JL. 2022. A new gas-accumulation theory of tight

sandstone gas accumulation in Turpan-Hami Basin-proximal-generation and proximal-storage type and self-generation and self-storage. Coal Science and Technology, 50(3), 176–186 (in Chinese with English abstract). doi: 10.13199/j.cnki.cst.2019-0691.

Pan R, Zhu XM, Tan MX, Zhang JF, Li Y, Di HL. 2018. Quantitative research on porosity evolution of deep tight reservoir in the Bashijiqike Formation in Kelasu structure zone, Kuqa Depression. Earth Science Frontiers, 25(02), 159–169 (in Chinese with English abstract). doi: 10.13745/j.esf.yx.2017-6-6.

Philp P, Symcox C, Wood M, Nguyen T, Kim D. 2021. Possible explantions for the predominance of tricyclic terpanes over pentacyclic terpanes in oils and rock extracts. Origanic Geochemistry, 155, 104220. doi: 10.1016/J.ORGGEOCHEM.2021.104220.

Samuel OJ, Kildahl-Andersen G, Nytoft HP, Johansen JE, Jones M. 2010. Novel tricyclic and tetracyclic terpanes in Tertiary deltaic oils: Structural identification, origin and application to petrpleum correlation. Org Geochem, 41(12), 1326–1337. doi: 10.1016/j.orggeochem.2010.10.002.

Segnit ER, Holland HD, Biscardi CJ. 1962. The solubility of calcite in aqueous solutions-I The solubility of calcite in water between 75° and 200° at $CO_2$ pressures up to 60 atm. Geochimica & Cosmochimica Acta, 26(12), 1301–1331. doi: 10.1016/0016-7037(62)90057-1.

Sun LD, Zou CN, Jin AL, Wei YS, Zhu RK, Wu ST, Guo Z. 2019. Development characteristics and orientation of tight oil and gas in China. Petroleum Exploration and Development, 46(6), 1015–1026. doi: 10.1016/S1876-3804(19)60264-8.

Sun LD, Cui BW, Zhu RK, Wang R, Feng ZH, Li BH, Zhang JY, Gao B, Wang QZ, Zeng HS, Liao YH, Jiang H. 2023. Shale oil enrichment evaluation and production law in Gulong Sag,Songliao Basin, NE China. Petroleum Exploration and Development, 50(3), 505–519. doi: 10.1016/S1876-3804(23)60406-9.

Tao SZ, Hu SY, Wang J, Bai B, Pang ZL, Wang M, Chen YY, Chen Y, Yang YQ, Jin X, Jia JH, Zhang TS, Lin SH, Meng YL, Liu HR, Wang L, Wu YY. 2023. Forming conditions, enrichment regularities and resource potentials of continental tight oil in China. Acta Petrolei Sinica, 44(8), 1222–1239 (in Chinese with English abstract). doi: 10.7623/syxb202308003.

Tong XG, Guo BC, Li JZ, Huang FX. 2012. Comparison study on accumulation & distribution of tight sandstone gas between China and the United States and its significance. Engineering Sciences, 14(6), 9–16 (in Chinese with English abstract). doi: 10.3969/j.issn.1009-1742.2012.06.002.

Wan JL, Gong YJ, Huang WH, Zhuo QG, Lu XS. 2022. Characteristics of hydrocarbon migration and accumulation in the Lower Jurassic reservoirs in the Tugerming area of the eastern Kuqa Depression, Tarim Basin. Journal of Petroleum Science and Engineering, 208, 109748. doi: 10.1016/J.PETROL.2021.109748.

Wang K, Zhang RH, Yu CF, Yang Z, Tang YG, Wei HX. 2020. Characteristics and controlling factors of Jurassic Ahe reservoir of the northern tectonic belt，Kuqa Depression, Tarim Basin. Natural Gas Geoscience, 31(5), 623–635 doi: 10.11764/j.issn.1672-1926.2020.04.005.

Wei GQ, Li J, Xie ZY, Yang W, Wang DL, Zhao ZH. 2013. Reservoir geology and exploration theories of large gas fields in China. Acta Petrolei Sinica, 34(S1), 1–13 (in Chinese with English abstract). doi: 10.7623/syxb2013S1001.

Wei GQ, Zhang RH, Zhi FQ, Wang K, Yu CF, Dong CY. 2021. Formation conditions and exploration directions of Mesozoic structural-lithologic stratigraphic reservoirs in the eastern Kuqa depression. Act Petrolei Sinica, 42(9), 1113–1125 (in Chinese with English abstract). doi: 10.7623/syxb202109001.

Zhang RH, Rong H, Zeng QL, Wang K, Wang JP, Meng GR, Li XJ. 2020. New progress in the theory and technology of tectonic diagenesis on reservoir and the geological significance of ultra-deep oil and gas exploration. Acta Petrolei Sinica, 41(10), 1278–1292 (in Chinese with English abstract). doi: 10.7623/syxb202010012.

Zhao CJ, Jiang YL, Liu JD, Wang LJ, Zeng T. 2021. A recovery method of porosity evolution based on forward and inverse analyses: a case stady of the tight sandstone of Xujiahe Formation, Northeast Sichuan Basin. Acta Petrolei Sinica, 42(6), 708–723 doi: 10.7623/syxb202106002.

Zhao HT, Sun Q, Li WH, Gao DK, Zhao FY, Lu SF, Zhu PF. 2022. Cretaceous hydrocarbon accumlation rules of the Yingmaili area in the Tabei uplift: A case study of the Yingmai 46 well block. Journal of China University of Mining & Technology, 51(01), 137–147 (in Chinese with English abstract). doi: 10.13247/j.cnki.jcumt.001304.

Zhi FQ, Zhang RH, Yu CF. 2023. Jurassic petroleum geological conditions and exploration directionin Yangxia Sag, eastern Kuqa Depression. Marine Origin Petroleum Geology, 28(02), 186–195 (in Chinese with English abstract). doi: 10.3969/j.issn.1672-9854.2023.02.008.

Zhu YM, Weng HX, Su AG, Liang DG, Peng DH. 2005. Geochemical characteristics of tertiary saline lacustrine oils in the Qaidam Basin. Chinese Journal of Geology, 20(10), 1875–1889. doi: 10.1016/j.apgeochem.2005.06.003.

Zhu YM, Hao, F, Zou, HY, Cai XY, Luo Y. 2007. Jurassic Oils in the Central Sichuan basin, Southwest China: Unusual Biomarker Distribution and Possible Origin. Organic Geochemistry, 38(11), 1884–1896. doi: 10.1016/j.orggeochem.2007.06.016.

Zou CN, Yang Z, He DB, Wei YS, Li J, Jia AL, Chen JJ, Zhao Q, Li YL, Li J, Yang S. 2018. Theory, technology and prospects of conventional and unconventional natural gas. Petroleum Exploration and Development, 45(4), 604–618. doi: 10.1016/S1876-3804(18)30066-1.